Universidade de Aveiro Departamento de Electrónica, Telecomunicações e Informática,
2016

Carla Iolanda Costa Rodrigues

Circuitos Óticos Integrados para NG-EPON

Photonic Integrated Circuits for NG-EPON

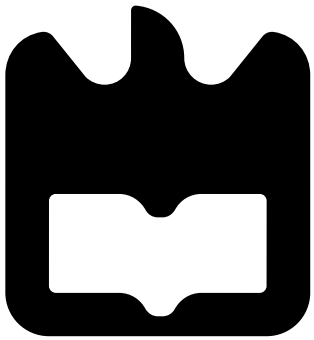

Carla Iolanda Costa Rodrigues

Circuitos Óticos Integrados Para NG-EPON

Photonic Integrated Circuits for NG-EPON

Dissertação apresentada à Universidade de Aveiro para cumprimento dos requisitos necessários à obtenção do grau de Mestre em Engenharia Electrónica e Telecomunicações, realizada sob a orientação científica de Dr. Mário Lima e Dr. António Teixeira, Professores do Departamento de Electrónica, Telecomunicações e Informática da Universidade de Aveiro.

Dedico este trabalho aos meus pais e irmão.

o júri / the jury

presidente / president

Professor Doutor Paulo Miguel Nepomuceno Pereira Monteiro
Professor Associado da Universidade de Aveiro

vogais / examiners committee

Professor Doutor Mário José Neves de Lima
Professor Auxiliar da Universidade de Aveiro (orientador)

Professora Doutora Maria do Carmo Raposo de Medeiros
Professor Associado da Universidade de Coimbra

agradecimentos

É com enorme satisfação que dedico este capítulo a todos os que contribuíram para o meu sucesso.

Começo por agradecer aos orientadores, Prof. Mário Lima e Prof. António Teixeira, pela transmissão de conhecimentos, disponibilidade, autonomia, bem como confiança que em mim depositaram.

Agradeço ao grupo de ótica que me acompanhou ao longo deste ano. Obrigada pela interajuda, partilha e trabalho de equipa.

Francisco, a tua boa vontade não vem de agora. Desde cedo que mostraste ser uma pessoa acessível e amiga. Quero-te agradecer pela amizade, paciência e profissionalismo, pois foste um pilar não só comigo mas de quem me é próximo. Motivaste-me e ajudaste a quebrar barreiras na realização desta dissertação. És um exemplo a seguir tanto a nível profissional como pessoal. Obrigada!

A todos os meus amigos que foram como uma família ao longo deste percurso. Caminhamos juntos e foram muitos os momentos que ficam para recordação. Desejo manter-vos sempre por perto.

Especial agradecimento às pessoas mais importantes da minha vida, os meus pais e irmão. Para além do amor, apoio incondicional, e valores transmitidos, foram eles que me proporcionaram todas as ferramentas necessárias para a conclusão desta etapa. Obrigada, por nunca deixarem de acreditar em mim.

Ao João agradeço pela força incansável em todos os momentos. Obrigada por me acompanhares durante todo este caminho, por seres a fonte de confiança e por todo o carinho demonstrado.

palavras chave Comunicações Óticas, NG-EPON, Transrecetor, PIC

Resumo

Em par com a privacidade e segurança, a crescente procura do consumidor por maiores larguras de banda apresenta um dos mais importantes desafios modernos das infraestruturas de telecomunicações. Esta procura incentiva assim a investigação de novas soluções não só eficientes, mas também economicamente viáveis, capazes de satisfazer as crescentes necessidades do consumidor. As comunicações óticas apresentam ser o meio apropriado para acompanhar este crescimento.

A Rede Óptica Passiva (PON) é uma arquitetura usada para distribuição de fibra ótica até ao consumidor final. Esta tecnologia permite dividir a largura de banda de uma única fibra por diferentes clientes. Tem havido um estudo constante no âmbito deste tópico para conseguir tirar máximo partido das capacidades da fibra e de modo a encontrar novas soluções para tornar este método mais simples.

Os Circuitos Óticos Integrados (PIC) são uma tecnologia que surge para ajudar na complexidade do *hardware* existente hoje em dia. Consiste num único *chip* capaz de integrar vários componentes óticos, o que leva a uma diminuição da complexidade, tamanho e redução do consumo de energia. Estas características fazem com que seja uma tecnologia vantajosa para uso em diferentes aplicações.

O desenho e a implementação da arquitetura do transrecetor em formato PIC no contexto da *Next Generation of Ethernet Passive Optical Network* (NG-EPON), é o principal objetivo desta dissertação onde visa o desenvolvimento circuitos óticos integrados para redes óticas de acesso futuras. Esta arquitetura deverá ser utilizada como *Optical Network Unit* (ONU) contendo 4 canais para atingir 100 *Gb/s*. Este trabalho contribuiu para o projeto FUTPON suportado pelo P2020.

keywords Optical Communications, NG-EPON, Transceiver, PIC

Abstract

Along with privacy and security, the growth of demand from the consumer for higher bandwidth presents one of the most important modern challenges in telecommunications infrastructures. The researchers were encouraged to find not only efficient but also the economically viable solutions capable of meeting the growing needs of the consumer. Optical communications are the way that can accompany this growth.

The Passive Optical Network (PON) is an architecture that shares the fiber bandwidth among several users. There has been a constant study under this topic for the purpose of using all the fiber abilities and to find new solutions to keep the access network simple.

Photonic Integrated Circuits (PICs) are a technology that emerged to help the complexity of the hardware that exists nowadays. It is a single chip capable of integrating numerous optical components, which leads to a reduced complexity, size and power consumption. These are the important characteristics that make the PICs a powerful tool to use in several applications.

This dissertation presents a monolithic PIC transceiver in the context of Next Generation of Ethernet Passive Optical Network (NG-EPON) which aims to design and implement integrated optical circuits for future access networks. The transceiver architecture is able to be used as an Optical Network Unit (ONU) with a 4 channels approach for 100 *Gb/s* solutions. The present work contributed for the FUTPON project supported by P2020.

Contents

List of Figures

List of Tables

Acronyms

1G-EPON	1 Gb/s ethernet passive optical network
10G-EPON	10 Gb/s ethernet passive optical network
AWG	Arrayed waveguide grating
BER	Bit error ratio
BB	Building block
B2B	Back-to-back
CD	Chromatic dispersion
CW	Continuous wave
DBR	Distributed Bragg reflector
DFB	Distributed feedback
DRC	Design rule check
EPON	Ethernet passive optical network
FEC	Forward error correction
FP	Fabry-perot
FhG-HHI	Fraunhofer heinrich hertz institute
FPR	Free propagation region
FSAN	Full service access network
FSR	Free spectral range

FTTx	Fiber-to-the-X (home, business, etc.)
HFC	Hybrid fiber coax
IEEE	Institute of electrical and electronics engineers
IC	Integrated circuit
IP	Internet protocol
InP	Indium phosphide
MMI	Multimode interference
MPW	Multi-project wafer
MQW	Multiquantum well
MZM	Mach-Zehnder modulator
NG-EPON	New generation of ethernet passive optical network
NRZ	Non-return to zero
ODN	Opical distribution network
OEO	Optical to electrical to optical
OLT	Optical line terminal
ONU	Optical network unit
OOK	On-off keying
PAM	Pulse amplitude modulation
PDK	Process design kit
PIC	Photonic integrated circuit
PIN	p-i-n photodiode
PON	Passive optical network
PMP	Point-to-multi-point

RZ	Return to zero
Si	Silicon
SNR	Signal-to-noise ratio
SOA	Semiconductor optical amplifier
SSC	Spot size converter
TW	Travelling-wave
xDSL	Digital subscriber loop
WDM	Wavelength division multiplexer

Chapter 1

Introduction

This chapter discusses the topic and scope of this work. Section 1.1 contextualizes and sets the motivation of the dissertation. Section 1.2 presents the main objectives. Right after, Section 1.3 exposes the structure of this work and in last, Section 1.4 lists the major contributions.

1.1 Overview and Motivation

The internet became an essential quotidian aspect in human lives driven by the necessity of connectivity between people. Nowadays, telecommunication networks are the most efficient and effective way to communicate at a distance. Due to the significant growth of these technologies over the years, it is necessary to increase the bandwidth and the speed of the internet. This demand poses one of the biggest challenges to internet providers as they require solutions capable of fulfilling these needs while maintaining their cost competitiveness.

Currently, the optical communications are the solution that provides the desired transmission capacity to the customers. This technology supports bit-rates in order of Terabits with long transmission distances. Thus, it contributed to one of the greatest revolutions of telecommunications in the last decades. It is necessary to keep investing on research for new solutions to address the growth of demand.

Different solutions for the access network have been under development for several years. The most important among these solutions are Digital Subscriber Loop (xDSL), Hybrid Fiber Coax (HFC), and Fiber-to-the-X (FTTx) i.e., to the premise, curb, home [1]. FTTx based on a passive optical network (PON) is considered to be the ultimate goal of the access networks since there are no limitations on both bandwidth and transmission length, contrary

to copper-based networks [2]. As the name suggests, this network is made of passive elements (with the exception of the terminal equipment). Hence, the transmission system does not require any use of energy, allowing a simplified network planning, cost reduction of operation and maintenance.

The New Generation of Ethernet Passive Optical Network (NG-EPON) is an evolution of the Ethernet Passive Optical Network (EPON) technology where the services are implemented based on Ethernet networks. This new technology appeared to helping fulfilling market demands. It is expected that NG-EPON is capable of providing up to 100 Gb/s in upstream and downstream directions.

The increasing demand for network bandwidth and quality of service caused a need for improvement on devices level. In this context appears the Photonic Integrated Circuit (PIC) that enables reduced power consumption and size compared to the hardware commonly used nowadays. PICs are considered as the way to make photonic systems or subsystems cheap and ubiquitous [3]. Optical elements are integrated on a small scale, such as lasers, modulators, optical amplifiers and multiplexers. These are the evolution in the optical domain, much like Integrated Circuits (IC)s were for electronics [3].

With this brief contextualization, the present dissertation intends to propose a PIC for NG-EPON usage, contributing to the development of those technologies. The integrated photonic transceiver developed on this work is intended to be used as an an Optical Network Unit (ONU).

1.2 Objectives

The aim of this work is to suggest an architecture and implement an integrated photonic transceiver for NG-EPON. So, the defined objectives for this thesis are the following:

- Simulate and test a transceiver with two different intensity modulation formats;
- Analyse and characterize several components from Fraunhofer Heinrich Hertz Institute (FhG-HHI) that are going to be used in the transceiver;
- Proposed a transceiver architecture;
- Develop the final mask layout.

1.3 Structure

Apart from this introductory chapter, this document is divided into six main Chapters, plus Appendices and it is presented as follows:

- **Chapter 2 - Passive Optical Networks and Photonic Integrated Circuits** gives the reader the main idea of a passive optical network architecture, followed by an approach about the NG-EPON and finishing with a vision about the photonic integrated circuits as well as the principle of operation regarding some optical components.

- **Chapter 3 - System Test: Modulation Formats** contains some simulations that were implemented to perform a transceiver functionality (transmission and reception) with different types of intensity modulation: Non-return to zero On-Off keying (NRZ-OOK) and Pulse Amplitude Modulation (4-PAM), using VPIphotonics^{TM}. The differences between these two modulation formats are compared according to the sensitivity and other aspects.

- **Chapter 4 - Study of Photonic Integrated Components** characterize various building blocks. It presents several studies to analyse the optical components' performance from the Fraunhofer Heinrich Hertz Institute's foundry. Those tests were made using a toolkit from VPIphotonics^{TM}.

- **Chapter 5 - Development of the Transceiver Architecture** exposes the procedure done to present the final purpose of the transceiver. It starts with a block diagram showing the overall architecture. Then, all the steps are described and, subsequently, the design of the PIC layout using PhoeniX Software's OptoDesigner is presented.

- **Chapter 6 - Conclusions and Future Work** closes this dissertation. It provides a description of the work done, as well as the main conclusions drawn from it. It is also listed some future work suggestions to develop in this research area.

1.4 Contributions

The principal contributions of this work are:

- Development of an ONU transmitter and receiver for NG-EPON;
- Design of a photonic integrated circuit;
- P2020 FUTPON project supported by P2020;
- Submission of the paper for *III International Conference on Applications in Optics and Photonics*, "Photonic Integrated Circuits for NG-EPON": Carla Rodrigues, Francisco Rodrigues, Mário Lima and António Teixeira.

Chapter 2

Passive Optical Networks and Photonic Integrated Circuits

Chapter 2 is divided into four sections. This chapter intends to provide the context and state of the art related to the topic of this dissertation. The overview of the PON architectures is going to take place in Section 2.1. Then, the NG-EPON networks are presented in Section 2.2, where it is also explained the market trends for this kind of technology. Right after, in Section 2.3 several optical components are described and a theoretical explanation of their operation principle it is given as a way of introducing complex topics in later chapters. The last Section 2.4 is devoted to PICs and their evolution.

2.1 PON Architecture

Passive optical network technologies are available since the mid-1990s where the Full Service Access Network (FSAN) consortium studied the feasibility of providing the fiber optics access service to end users. Since then, and specially in the last few years, these have been improved and extended with commercial standards being implemented [4]. Due to the need for higher bandwidth and trying to balance with operational costs, PONs have become the major topology currently used in optical communications architectures. PON a point-to-multipoint topology which provides broadband access. There are a number of PON-based access architectures providing connectivity between the Optical Line Terminal (OLT) and the demarcation point, the Optical Network Unit (ONU). Depending on the actual location of the ONU, there are several classes of fiber access networks, namely FTTx where the X denotes: curb/cabinet, building, desktop, home [5].

Figure 2.1 represents a PON architecture. The OLT and the ONU are the only active components of a PON network. The OLT consists of the device that transmits and receives data to and from the users. The ONU is the device that terminates the network at the user side. These two devices are the only active elements. Is important to refer that connection between the OLT and the ONU is designated as Optical Distribution Network (ODN), an optical fiber structure which can be defined according to the way it reaches the ONU. Each ODN has two different types of transmission: the upstream and the downstream. The downstream is the direction that goes from the OLT and is received in the ONU side. Unlike the downstream, the upstream direction transmits the signal from the ONU and goes to the receiver, the OLT [4].

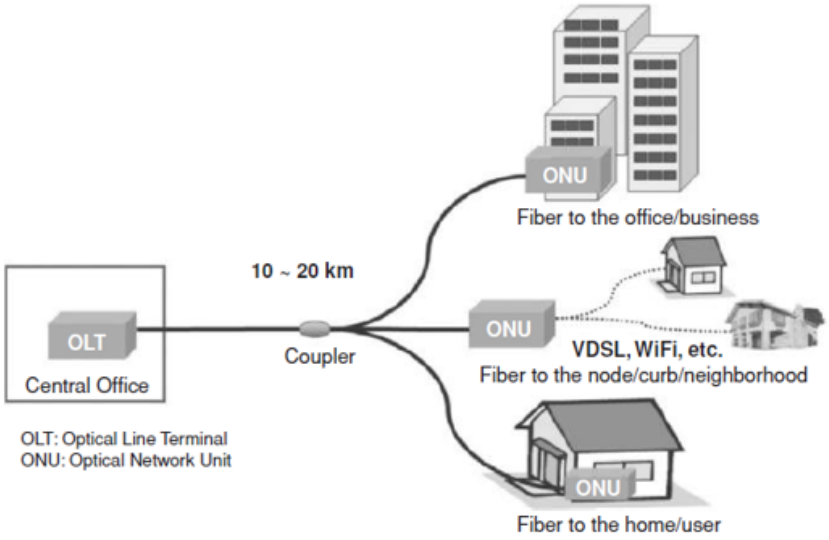

Figure 2.1: Example of a PON-based access architecture [4].

Given the higher development of those technologies, PON standardisation activities have been ongoing for the past fifteen years within the Telecommunication Standardization Sector of the International Telecommunication Union (ITU-T) and the Institute of Electrical and Electronics Engineers (IEEE) standards bodies.

2.2 Next Generation of EPON

In 2001, a group created by IEEE 802.3ah called *Ethernet in the First Mile Task Force* brought the notion of EPON architecture. Since a big percentage of data traffic is done by

using Ethernet frames it was reasonable to create a PON architecture based on that. As so, the aim of this architecture was to transport all the information through Ethernet frames until the area of the user access. EPON, also referred as 1G-EPON, is a native Ethernet solution that leverage the features, compatibility, and performance of the Ethernet protocol. It is an architecture operating at the effective data rate of 1 *Gb/s* in both downstream and upstream directions [5] and it was created to support point-to-multipoint (PMP) connectivity over the Ethernet technology, where the Ethernet traffic is transported natively, and all features are fully supported [6]. EPON is less popular in Europe and in United States of America, but is dominant in Japan and South Korea.

EPON is a optical network that can be considered a fiber access network. As a PON technology, this architecture does not contain active elements in the outside plant. The passive elements are placed between the OLT and the ONU: the single mode fiber and the passive optical splitters that divide the signal to the end users.

In December of 2004, with some tests done on 1G-EPON (First generation of EPON), this topology quickly emerged as the market-leading optical access technology in multiple application areas in different points around the world [5].

China Telecom started to test and deploy EPON network in 2005. Then, the enterprise presented more than 60 million subscribers in 2007, having a major market growth and achieving great speed using the FTTx networks [5].

10G-EPON was developed to guarantee the compatibility with the existing 1G-EPON in various countries but to allow higher bitrates. This architecture uses the Ethernet stack, and it has two modes of operation: symmetric and asymmetric. In the symmetric operation, it supports both downstream and upstream data paths operating at 10 *Gb/s*. However, in the asymmetric mode, it holds 10 *Gb/s* in the downlink and 1 *Gb/s* in uplink. This standard was issued in 2009 by IEEE 802.3av group [5].

The research on next generation PONs are focused in finding solutions to allow higher bandwidths for both downstream and upstream transmissions. Nowadays, there are a major development efforts focused on EPON topologies. NG-EPON appeared as an evolution of the standards 1G-EPON and 10G-EPON. The main goals for this architecture is to have a relation between lower cost, more users and higher bandwidth. In this architecture, the user is given all the information via Internet Protocol (IP). It is predicted that NG-EPON will allow up to 100 *Gb/s* of speed on symmetric and asymmetric mode.

This networks presents several advantages besides the bitrate, such as the capacity of

changing the split ratio on ODN and coexistence with other networks types already implemented. The residential and business users are the two general classes of users foreseen for NG-EPON. Residential users tend to use data services asymmetrically and tolerate best-effort delivery, whereas premium/business subscribers demand dedicated symmetrical data rates [5].

This research is being done by the IEEE 802.3 Ethernet Working Group which presented an ad hoc where the scope was on gathering information to see the requirements, the feasibility, and others aspects regarding the whole architecture [5].

2.3 Optical Components

Study of different components is a relevant step for designing a PIC. Nowadays, a right choice of a certain component is a key for better results in the integration. There has been a constant research under this topic to improve the characteristics of the components as well as finding new applications for them. Section 2.3 presents several optical components that are going to be used to perform the transceiver architecture. A brief explanation of the operational principle for each of them is introduced and their main features are described.

2.3.1 Distributed Feedback Laser (DFB)

Wavelength tunable laser is a promising light sources for future Wavelength Division Multiplexer (WDM) networks [7]. The Distributed Feedback (DFB) lasers and the distributed Bragg reflector (DBR) are, nowadays, the best candidates to perform as light sources in monolithically integrated devices since they have an high-speed direct modulation characteristic, hold tunable capacities and present a great single-mode behaviour with a small spectral width (in order of a few MHz) [8].

To understand how a laser produces light, it is important to consider the three fundamental processes in a semiconductor laser: the absorption, the spontaneous emission and stimulated emission. These main processes behind laser operation can be seen in Figure 2.2.

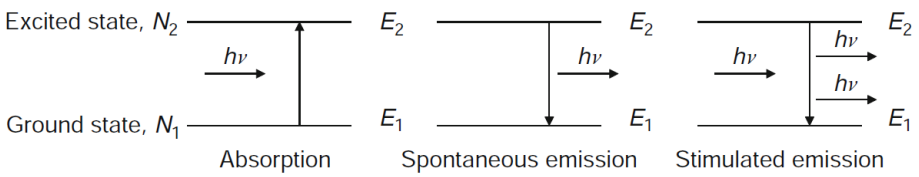

Figure 2.2: Schematic illustration of the three main processes: absorption, spontaneous emisson and stimulated emission, respectively [9].

The absorption case, related to the a) part of the Figure 2.2, happens when a photon's energy is absorbed by an electron in state E_1 (known as ground state), thus exciting it to the state E_2 (called as excited state) [10].

In the case of Figure 2.2 b), which relates to the spontaneous emission, the electron in the excited state E_2 can spontaneously decay to the state E_1, and a photon will be generated if hv is higher than $E_2 - E_1$. The light provided by the spontaneous emission has random propagation direction, random phase, random frequency and it has wide linewidth [10].

The stimulated emission, referred to Figure 2.2 c), occurs when a photon with proper energy ($hv > E_2 - E_1$), unleash to a stimulated recombination of a carrier from the ground state (E_1) with a hole from the excited state (E_2), and an identical photon to the initial one is formed. The produced light is coherent in this case.

The last process that was mentioned, the stimulated emission, is the main principle behind lasers. In order to have gain, most of the electrons need to be in the state E_2, so there is a population inversion, achieved by electrical pumping [11].

The structure of a DFB laser is represented in the following Figure 2.3.

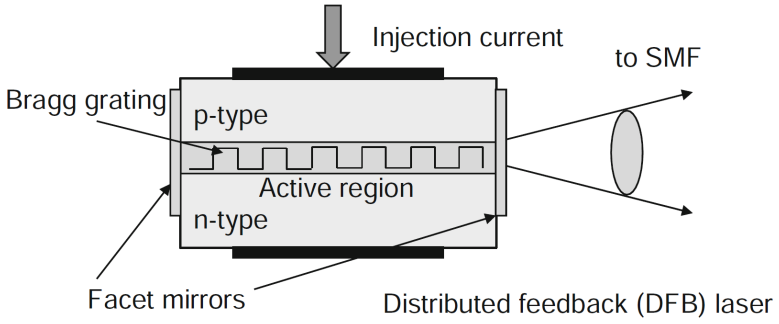

Figure 2.3: Schematic diagram of a DFB laser [9].

The DFB lasers, have a thin active region between the p and n type layers, where it appears a grating cavity. The feedback mechanism is distributed throughout this cavity, and

it provides a periodical variation of the waveguide refractive index. This leads to creating waves that propagate in forward and backwards directions and they are coupled with each other. The selection of a particular mode depends on the grating period and in the average mode index. In conclusion, the grating cavity works as the wavelength selective element [8].

The temperature is the key factor to the emission wavelength. This dependence leads to the tunability of these lasers, which is the main feature of WDM systems. The temperature is changed by the injection of current through the laser. This current goes to a resistor where it causes heating and this process will lead to more output power. Because of this thermal dissipation, the volume of the laser cavity will change as well as the refractive index, resulting in a change of the wavelength [7].

There is a relationship between the output power with the current injected. This behaviour is exposed in Figure 2.4.

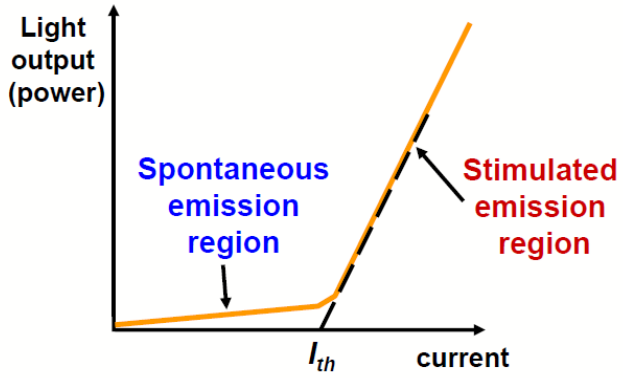

Figure 2.4: The light output against current characteristic for an injection laser [10].

The *P-I* curve, that is represented in Figure 2.4, characterize the emission properties of a semiconductor laser, since it indicates where is the threshold level and the current needed to obtain certain value of output power [12].

Initially, with low values of current, the laser emits in the spontaneous emission. However, when it rises to the threshold current, I_{th}, there is a fast transition between spontaneous and stimulated emission that leads to a higher light output. The optical output power rises steeply with increasing current.

The threshold current increases with p-n junction temperature so, it has a temperature dependence. This relationship is obtained by:

$$I_{th} = I_0 \epsilon^{\left(\frac{T}{T_0}\right)}, \tag{2.1}$$

Where I_0 and T_0 are constants and T is the temperature. Resuming, the graph is shown in Figure 2.4 will be changing according to the temperature.

2.3.2 Semiconductor Optical Amplifier (SOA)

This component is one type of amplifier in the optical domain. It is similar to its electrical one because also amplifies the signal, there is noise added to the amplified signal and the gain/noise can be measured and calculated. The main difference is about bandwidths that each of them provide. In case of the optical amplifier, it provides wide spectral bandwidths.

The research on semiconductor optical amplifiers started soon after the invention of semiconductor lasers in 1962. However, it was only during the 1980s that SOAs were developed for practical applications, motivated largely by their potential applications in lightwave systems [12].

Nowadays, the SOA is a key element of PIC technology because it offers low input power requirements, large gain, large optical bandwidth, very short response times and it is a very compact device. Moreover, they are cheap and have different applications, including in optical switches, modulators, wavelength converters and in the integration with other active or passive optical components. It presents some advantages in the transmission part (increasing the power of the signal), in the reception part (increasing the sensitivity of the photodetector) and in the fiber (decreasing the losses).

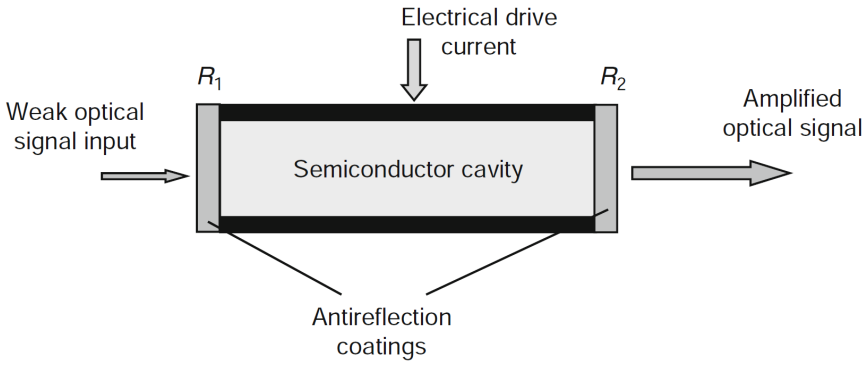

Figure 2.5: Structure of SOA [9].

Figure 2.5 describes the operational principle of this component. The input signal goes through an active region. An external injection current acts as an energy source that enables pumping electrons to the conduction band. Then, there is a transition from the conduction band to the valence one. This phenomenon, known as stimulated emission, generates

an amplified output signal. However, the output signal has additive noise, produced by the amplification process and cannot be fully avoided [13].

The SOAs are classified in two different regimes of operation:

- Fabry-Perot (FP): the device has facets that partially reflects the light;
- Travelling-Wave (TW): the light propagates once in the gain surface.

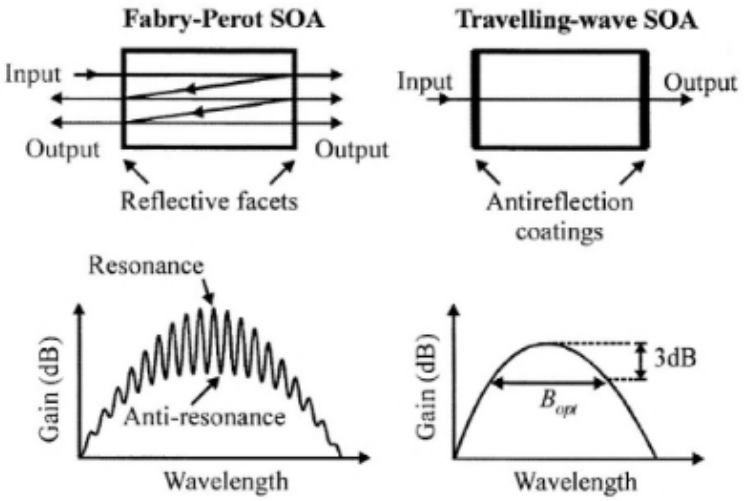

Figure 2.6: Basic types of SOA and related gain spectrum [13].

The difference between the structure of the two mentioned types of SOA and how the gain behaves along the wavelength spectrum are showed in Figure 2.6. In the case of the left image from Figure 2.6, the Fabry-Perot SOA has reflective facets at the edges of the device, so the light travels through multiple pads. These reflectivity's facets produce the ripples in the gain spectrum, and this is why it is known as a resonant amplifier. Comparing to the Travelling-wave SOA, is more sensitive to variations in bias current, temperature and signal polarisation.

The Travelling-wave SOA, on the right part of the Figure 2.6, contains antireflection coatings at the end of the device, which makes the reflections negligible and the gain becomes smoother comparing to FP-SOA. Moreover, TW-SOA possesses bigger bandwidth and saturation power, it reduces the temperature and current density and because of this characteristics TW-SOAs are the most used nowadays. [13].

In general, when an optical amplifier is studied, the gain is another relevant feature. The gain of a SOA is the ratio between the output optical power and the input optical power. In the Figure 2.7, firstly there is a flat region, where the Small Signal Gain (SSG) is contained. and represents the maximum achievable gain of a determined amplifier, where the amplifier operates with a constant gain without any non-linear effects [14].

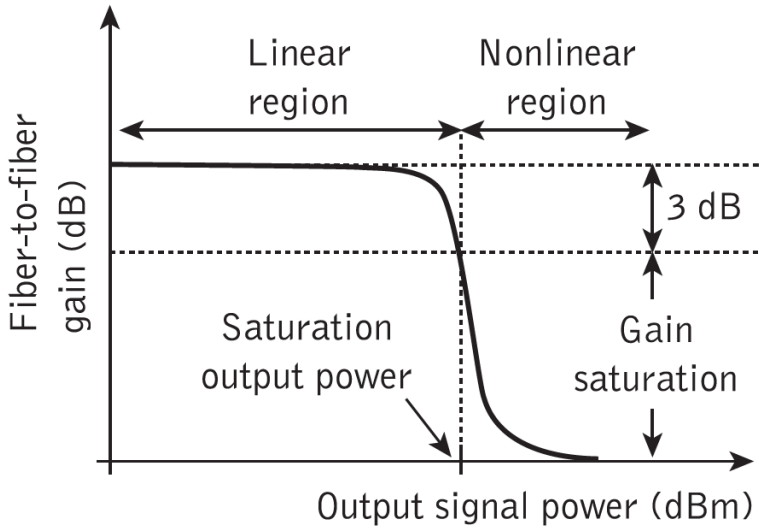

Figure 2.7: Gain over output power [15].

After that, saturation gain is reached. This happens in any amplifier when the input power increases too much and there are no more carriers available in the active region. When the input power is close to the saturation power (that causes the gain to fall 3 dB), the amplifier gain is not linear any more, and it decreases drastically.

Figure 2.8 shows a typical gain curve for an SOA with different biasing currents. For larger bias current the gain will increase as well until this growth starts to saturate at a certain point. Furthermore, for each bias current, the peak gain is different considering the wavelength.

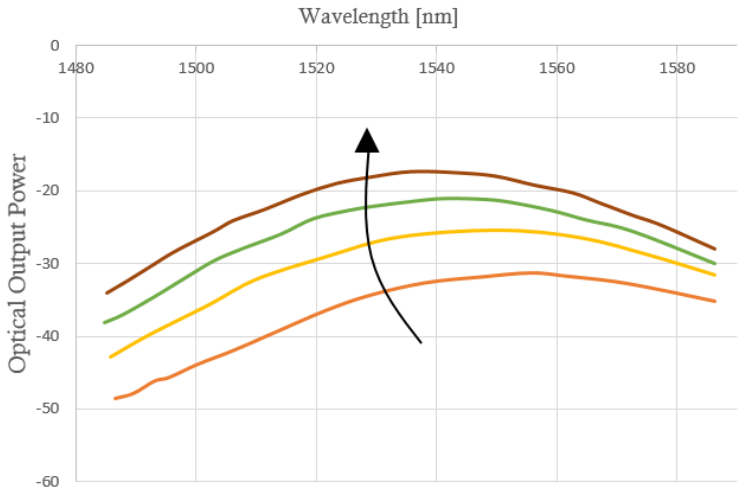

Figure 2.8: Optical power over wavelength for different values of bias current.

2.3.3 Array Waveguide Grating (AWG)

The Array Waveguide Grating (AWG) that it is also called as Phased Array (PHASAR) and Waveguide Grating Router (WGR), started to be researched since the early 1900's [16] by Smit. It is one of the most requested blocks in integrated optics since it can act as a multiplexer or demultiplexer providing wavelength filtering. There are several applications for this component besides the wavelength filtering such as signal processing, measurement, characterization or sensing [16].

The device is a passive optical component based on an array of waveguides in the input that are imaging onto an array of output waveguides [17]. The component started to be adopted with one input and N outputs, but since 1991, Dragone presented an evolution of it, presenting an AWG with N inputs and N outputs [16].

A schematic layout from an AWG can be seen in Figure 2.9. The image shows that this device holds the transmitter and receiver waveguides which means that it is connected to the input and output ports. These ports are connected to the Free Propagation Region (FPR) considered as the focusing slab regions. On the opposite side of the FPR, there is the aperture, which is the key to connecting to the phased arms of multiple channel waveguides.

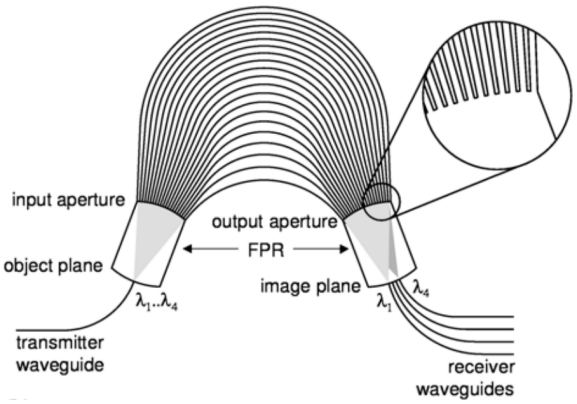

Figure 2.9: Layout of the AWG demultiplexer [16].

Basically, the light is propagated through the transmitter waveguide until it enters the FPR area and gets diffracted. In the input aperture, the beam is coupled into the array waveguide structure that guides the light in each wavelength until the output aperture, where the different waveguides are led to the different output ports.

Focusing the fields of propagation in an AWG, the length of the arms are determined by the path that each of them takes, ΔL. The focusing will happen if ΔL is given by an integer multiple of the central wavelength (λ_c) of the AWG, .

Due to the increase of the arms the separation between the adjacent waveguides is a phase difference of [16]:

$$\Delta\phi = \beta \times \Delta L, \tag{2.2}$$

where ΔL is the length between the waveguides that enables the focusing and β is the constant of propagation that is given by [16]:

$$\beta = \frac{2\pi\nu\eta_{eff}}{c}, \tag{2.3}$$

considering that ν is the frequency of the propagating wave, η_{eff} the effective refractive index of the waveguide and c as the speed of light in vacuum.

The FSR appears when the phase $\Delta\phi$ is equal to 2π, which means that the response of the AWG is periodic. This parameter is the period in the frequency domain and leads to the following expression [16]:

$$FSR = \frac{\nu_c}{m}\frac{\eta_{eff}}{\eta_g}, \tag{2.4}$$

in which m is an integer number that represents the order of the array waveguide and n_g is the group index mode of the waveguide.

This parameter is exposed in the next Figure 2.10. The frequency response of these filters is represented for different channels spaced by the chosen FSR.

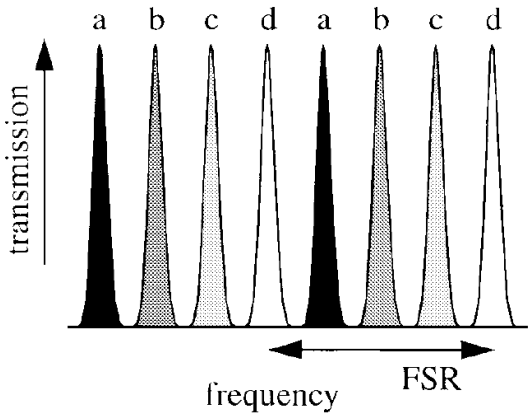

Figure 2.10: Frequency response of an AWG with the different channels [17].

Crosstalk is is very relevant and needs to be taken into account, since is caused by a contribution of an undesired signal in a channel. This phenomena can be caused by many mechanisms and is not limited by design but by imperfections from the fabrication process. AWGs based in InP devices have typical values of -25 dB of crosstalk [16].

It is important to refer that the better the device, the higher the crosstalk [16].

2.3.4 Photodetectors

The photodetectors represent the last stage of the reception part from a system. Their function is to detect the received optical signal, and they are responsible for converting it into an electrical one, so the information is recovered and sent to the destination. It is one of the most important components of an optical communication system so it should have high sensitivity, fast response, low cost and size, and large fidelity [18].

The principle of operation behind photodetectors is the internal photoelectric effect. The light is absorbed in a semiconductor for photo-generation of electron-hole pairs. For this to occur the photon energy hv should be greater than the band gap energy, E_g, of the material so then, the electron excites from the valence to the conduction band.

This separation between holes and electrons made by the electric field results in a flow of current (photocurrent I_p) in the circuit proportional to the incident optical power. The

photocurrent is written as follows [18]:

$$I_p = R \times P_{in}, \tag{2.5}$$

where R is the responsivity and P_{in} is the input power.

Responsivity is one of the main performance defining characteristics of the photodetectors. It is the ratio of output current to input optical power, specified in amperes per watt (A/W) and is dependant on the wavelength of the incident light as well as the applied bias voltage and temperature. Responsivity is expressed by the following formula [18]:

$$R = \frac{q\eta}{hf}, \tag{2.6}$$

where q is the electron charge, h the Planck's constant, f the photon frequency and η the quantum efficiency. Responsivity increases slightly with applied reverse voltage due to improved charge collection efficiency in the photodiode. The variations of the responsivity due to a change in temperature are caused by a decrease or increase of the band gap [12].

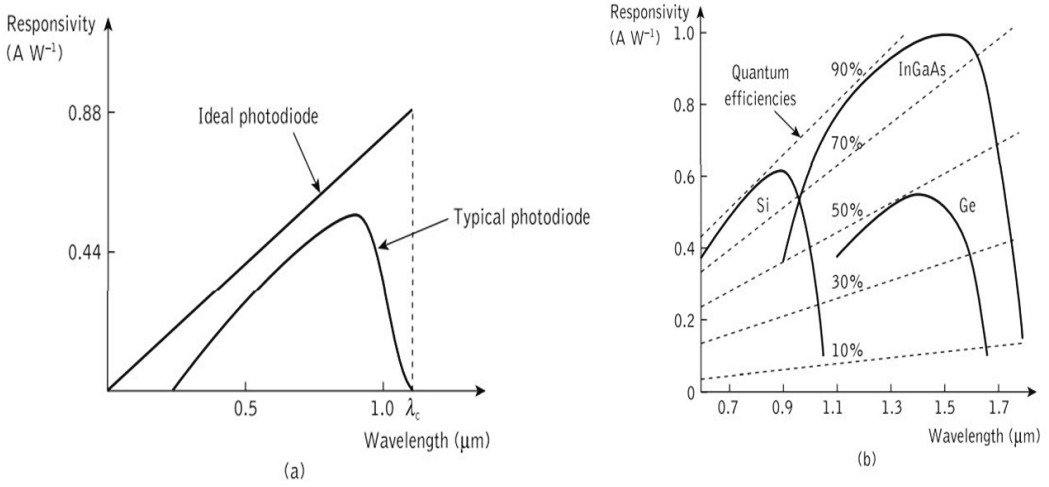

Figure 2.11: Responsivity as function as wavelength: (a) difference between ideal and typical photodiode; (b) responsivity of different semiconductors materials along the wavelength [18].

In Figure 2.11a, the responsivity is linearly dependent on the wavelength, λ, until a certain limit where the quantum efficiency, η, drops to almost zero. This occurs at cut-off wavelength (λ_c) and varies according to the semiconductor material as presented in Figure 2.11b.

Another relevant aspect to consider in photodetectors is the absorption, α. It was referenced before that the absorption of photons produces carriers pairs. This constant coefficient is strongly dependent on wavelength [15]. Consequently, it is also dependent on the semiconductors which offer different absorption coefficients as can be seen in the following Figure 2.12.

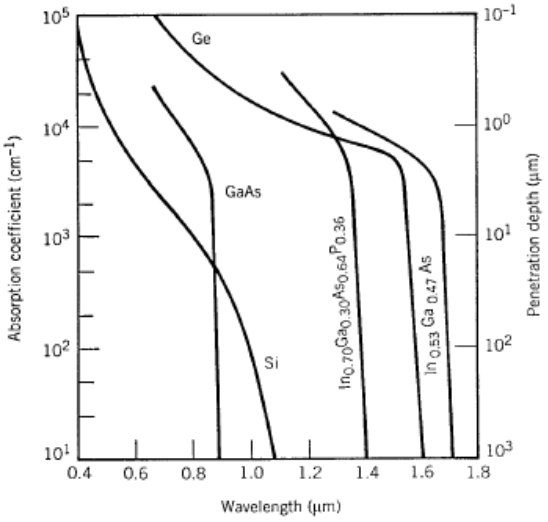

Figure 2.12: Wavelength dependence of the absorption coefficient for different semiconductors materials [12].

Figure 2.12 shows the wavelength dependence for different α coefficients commonly used in photodetectors. When α becomes zero it means that the cut-off wavelength was reached and the photodetector can only be used at $\lambda < \lambda_c$.

2.3.4.1 *p-i-n* Photodiode

PIN (denotes the p-intrinsic-n doping) is one of the main types of photodetectors. It consists of adding an intrinsic undoped semiconductor layer between p and n regions which it is represented in Figure 2.13. With this topology, the photodetector increases the depletion region width, the absorption of incident light and, improves the quantum efficiency of the photodetector [19].

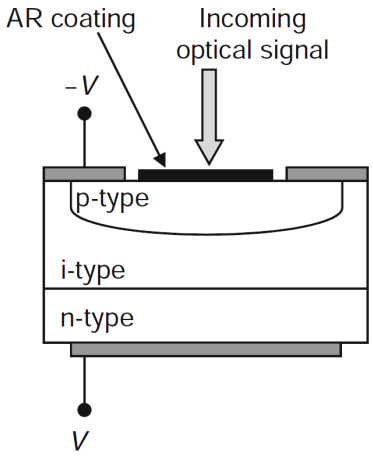

Figure 2.13: Structure of a *p-i-n* photodetector [9].

When photons have energy greater than the bandgap energy of the semiconductor, electron–hole pairs are generated in the depletion layer and, because of the high electric field in the depletion region, the electron-holes are separated and travel in different directions towards the p or n side which leads to an electric current flow [20].

2.4 Photonic Integrated Circuits (PICs)

In microelectronics, there is a clear exponential development in the number of transistors per chip, which has been doubling every two years on average during the last four decades. This phenomenon is known as Moore's law [21].

Nowadays, the electronic integrated circuits (ICs) are strongly being used and is difficult to imagine our lives without them. The integration was a revolution because it offers low cost, low size, and high performance. The optical integrated circuits, known as photonic integrated circuits (PICs), consist of the same technology as ICs but in an optical domain. Instead of having electrons flowing, there are photons that move through the waveguides. The main application of PICs are in fiber optic communications but, it is also possible to use this technology in photonic computing, sensing devices or in biomedicine.

PICs emerged to the necessity of increased robustness, security and offer a to decrease in price, size, and power consumption. The technology appeared in 60's but the era of high-complexity PICs started in 1988 when Smit [16] published the invention of the AWG presented in Section 2.3.3. However, only in 2005 an enterprise called Infinera presented the first PIC to be commercially available. It was a transceiver with WDM system. It had 10 channels

with more than 50 integrated components in a single chip.

PIC is a technology that has been adding points on the market where the lasers, modulators, detectors, amplifiers, are on a single chip. It simplifies the optical system design due to integration, reduces footprint, improves reliability and decreases the number of OEO (Optical-Electrical-Optical) conversions.

As it happens in electronic circuits, the photonic integration can be divided between both hybrid or monolithic integration. The hybrid integration has assembled optical devices into a single package, and can have electronic ICs associated. In another hand, the monolithic integration combines only multiple optical devices. The monolithic integration provides several benefits, starting on power consumption, the lower footprint, and more reliability [22].

Besides the type of integration for the PICs, differences also exist on the types of platforms available for the substrate materials. The main types used are: Silicon (Si), Indium Phosphide (InP) and TriPleX (combination of Silicon Nitride – Si_3N_4 and Silicon Dioxide – SiO_2). Nowadays, the market leaders are the Si and InP. Each platform has different performances according to their applications as can be seen in Figure 2.14

	Performance		
Building block	InP	Si	TriPleX
Passive components	●	●●	●●●
Lasers	●●●	○	○
Modulators	●●●	●●	●
Switches	●●●	●●●	●
Optical amplifiers	●●●	○	○
Detectors	●●●	●●●	○
Footprint	●●	●●●	●
Chip cost	●	●●	●●
CMOS compatibility	○○	●●	●
Low-cost packaging	○	○[1]/●●[2]	●●

Performance	
●●●	Very good
●●	Good
●	Modest
○	Challenging

Figure 2.14: Performance comparison of the three commercially available technology platforms: InP, Si and TriPleX [23].

Several European projects have been implementing the InP-based generic photonic integration technology, since it can integrate both active and passive optical devices. InP enables the monolithic integration unlike silicon that only allows the integration of passive devices due the difficulty on OEO conversions [22, 24].

Apart from the advantage presented before, InP is a material that is inserted in the JePPIX platform, in which Europe's key players are cooperating such FhG-HHI, Smart Photonics and Oclaro. This component is also integrated in the Multi-Project Wafer (MPW) where several

chips can be combined in the same wafer providing a low cost in the R&D phase and more functionalities on designing a PIC [25].

The market for integrated components is still small, but it is expected to become increasingly important in the coming years [17].

Chapter 3

System Test: Intensity Modulation Formats

In this Chapter some simulations are presented using VPIphotonics software to compare two modulation formats: Non-Return to Zero (NRZ)-OOK and Pulse-amplitude modulation (PAM). The Chapter starts with a brief outline of the differences between them. Right after, one channel system is simulated and the sensitivity is compared. Lastly, a four-channel system is presented and its performance is also tested.

3.1 Modulation Formats

The main goal of a modulation technique is to compress/compact the biggest amount of data into the smallest possible spectrum. As so, many techniques have arisen to improve the spectral efficiency, a measure of how fast the data can be transmitted in a determined bandwidth [26].

OOK is the dominant modulation format that is used in optical communications because of its easy implementation. There are two possible versions of OOK regarding the pulse format: Non-return to zero (NRZ) where the optical signal occupies the whole period of the bit and, Return to Zero (RZ), where it occupies just a portion of the bit period.

It is possible to encode more data into the same timeframe, however it is necessary to call on modulation formats with multiple distinct levels. The pulse amplitude modulation, PAM, is one of them.

As PAM it is a multi-level format, where (M-PAM) encodes M symbols in M different amplitudes, where M is equal 2^N, in which N correspond to the number of bits. So, actually,

the NRZ-OOK format is a two-level PAM system while, 4-PAM is a four level format. From now on, the NRZ-OOK is designated as 2-PAM. As example, Figure 3.1 shows three different constellation, transmitting 1 bit, 2 bits and 3 bits per symbol.

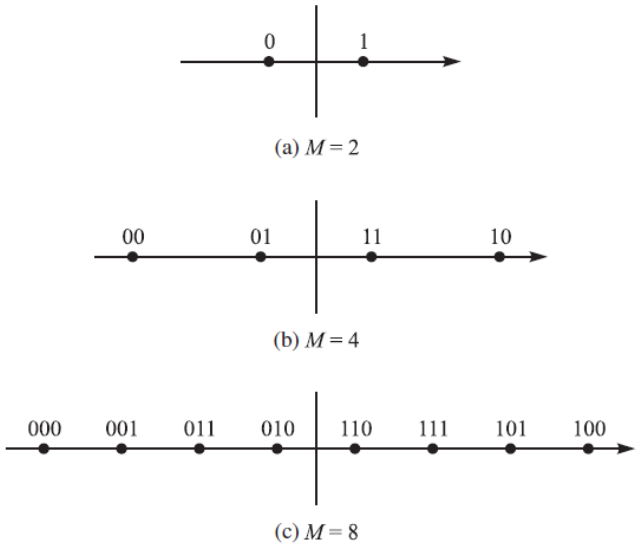

Figure 3.1: Constellation of M-PAM signal.

The 2-PAM encodes 1 bit per symbol and 4-PAM represents one symbol with 2 bits. As said, the 4-PAM has 4 levels to encode the symbols as the following image 3.2 shows. The spectral efficiency is then different. A multi-level modulation format is N times more efficient than a binary modulation format [27].

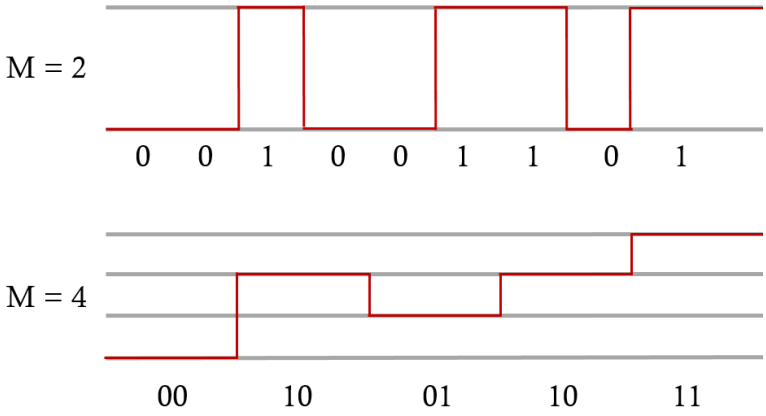

Figure 3.2: Example of a M-PAM signal.

It is reasonable to say that 2-PAM will need twice more bandwidth comparing to 4-

PAM. However, 4-PAM has a price to pay since it requires a higher Signal-to-Noise Ratio (SNR) because of the difference between levels is lower, and therefore, it presents a higher susceptibility to noise [28]. Despite this, 4-PAM has been a popular solution to the pluggable optical transceivers because of its simplicity of implementation and low power consumption.

3.2 2-PAM and 4-PAM Comparison

The comparison between these two modulation formats takes place in this Section 3.2. Firstly, the sensitivity of both modulation formats with only one channel and back-to-back (B2B), that means without fiber, is compared. Right after a fiber with different lengths was introduced and the sensitivity was analysed one more time. Then, three more channels were added and the same simulations were performed.

3.2.1 Receiver Sensitivity in Back-to-back

The primary factor that is going to be investigated in this system is the receiver sensitivity in a back-to-back setup. In that sense, Bit Error Ratio (BER) is defined as the number of bits with errors over the total number that was sent. This is commonly used as a figure of merit. The receiver sensitivity lets us know the minimum required optical power to keep the BER below a given value [12].

The signal power that arrives at the receiver is dependent on many factors, such as the optical signal strength and the photodetector used [20]. In this case, a PIN receiver was used with ideal parameters. The main factor to investigate is the optical signal that was modulated with 2-PAM and with 4-PAM.

The setup is demonstrated in Figure 3.3 where a back-to-back measurement can be founded. It begins with a module that implements a multilevel PAM electrical source. The number of levels is given by 2^N, where N is the number of bits per symbol, 1 in the case of 2-PAM and 2 in the case of 4-PAM. The electrical carrier comes from the laser that produces a continuous wave (CW) with an optical wavelength (1550 nm) and a power of 1 mW and goes through the Mach-Zehnder (MZM) to be modulated. The attenuator is the module to attenuate the optical signal and is followed by the receiver block. The receiver consists of a PIN photodetector that is an ideal one with no dark current and shot noise. The filter reduces the noise from the electrical signal. Lastly, there is a module that estimates the bit error ratio (BER) in transmission systems utilising multilevel modulation. The setup will display the

results as an XY plot, the 2D one.

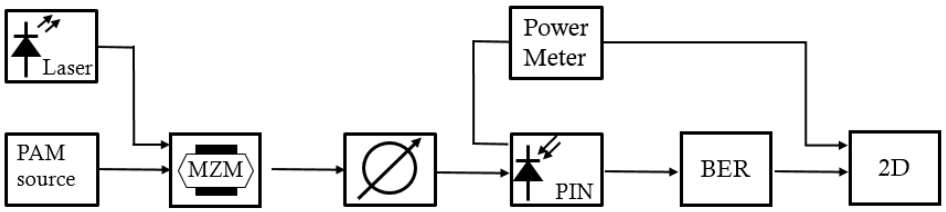

Figure 3.3: Setup used to test the sensitivity in back-to-back.

The logarithmic scale BER over the receiver power at the receiver is shown in Figure 3.4. Two different modulation formats are compared, 2-PAM and 4-PAM with the same baud-rate, 25 *Gbaud* which is equivalent to 25 *Gb/s* for 2-PAM and 50 *Gb/s* for 4-PAM .

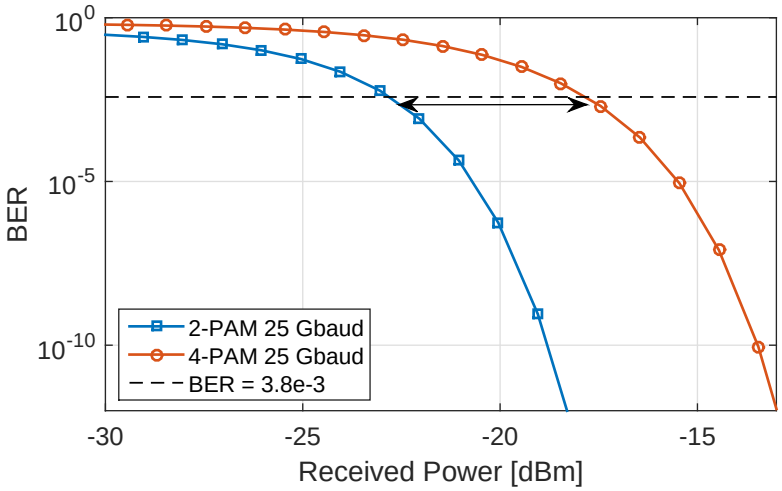

Figure 3.4: Received power of 2-PAM and 4-PAM for the same baud-rate.

The results from the simulation environment, presented in the previous graph, are in line with the expected.

The BER value of 3.8×10^{-3}, is the threshold BER in which using a Forward Error Correction FEC, the signal can achieve the 10^{-9} value. At this point, the received power for 25 *Gbaud* of 2-PAM is around -22.6 *dBm* and for 25 *Gbaud* of 4-PAM is approximately -17.7 *dBm*. The power penalty is around 4.9 *dB*.

The analytical value of the power penalty between different levels of modulation is given by:

$$Penalty(dB) = 10 \times \log_{10}(M-1), \tag{3.1}$$

where M consists of the levels.

It concludes that with 4 levels, like 4-PAM, the power penalty is, approximately, 4.8 dB which makes the simulation in line with the theory [5].

3.2.2 Receiver Sensitivity with different Fiber Lengths

As the name of this section indicates, the fiber was introduced after the MZM modulator, resulting in the setup presented in Figure 3.5.

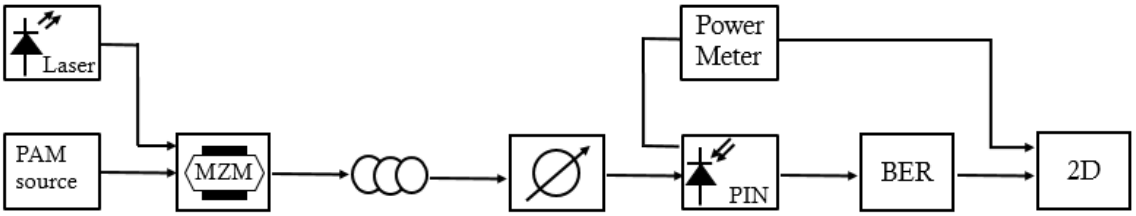

Figure 3.5: Setup used to test the sensitivity with different fiber lengths.

The lengths of fiber are from 0 to 40 km with increments of 5 km and the simulations were performed for 5, 10, 12.5, 20 and 25 $Gbaud$ of the symbol-rate. Adding the fiber component it was possible to characterize a system with other associated effects, like the chromatic dispersion (CD), which the value used was 16 $ps/nm/km$.

The results for the receiver sensitivity at BER of 3.8×10^{-3} for different fiber lengths are in the following Figure 3.6. Figure 3.6a is related to the 2-PAM modulation and the Figure 3.6b is about the 4-PAM.

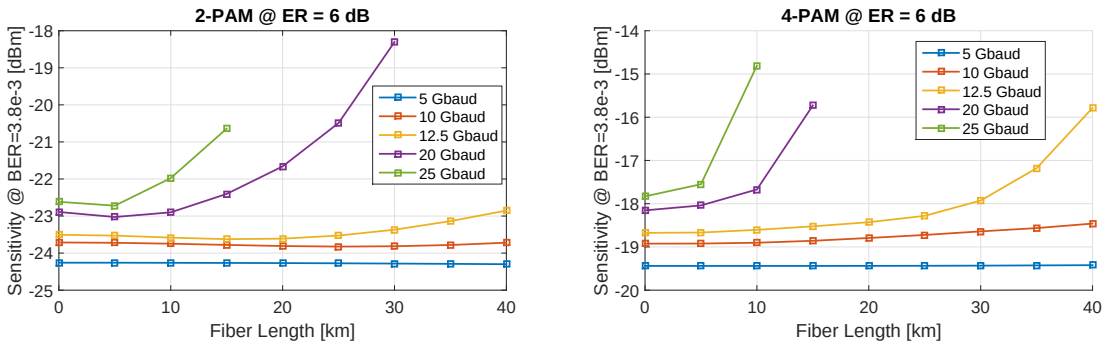

(a) 2-PAM modulation format

(b) 4-PAM modulation format

Figure 3.6: Variation of the sensitivity for different fiber lengths and baud-rate.

As referred before, since 4-PAM has four levels and encodes 2 bits per symbol, the baud-

rate is half of the bit-rate, however, in the 2-PAM modulation format the bit-rate leads to the same baud-rate because each symbol carries only one bit.

Another aspect relevant to mention is the chromatic dispersion. The chromatic dispersion is one of the major impairments that will deteriorate the optical signal since it leads to pulse broadening and inter symbol interference [20]. The total chromatic dispersion is dependent on the fiber length because CD is given in *ps/nm/km*. Increasing the length leads to an increase of the total chromatic dispersion. CD is caused by the different spectral components of the signal travelling in different speeds through the fiber.

With this overview, for the same baud-rate, the 4-PAM holds a worse behaviour because the inference between symbols are severest. To better understand this phenomenon, the same simulation was done, but now the methodology to be compared is in bit-rate. The results are in Figure 3.7.

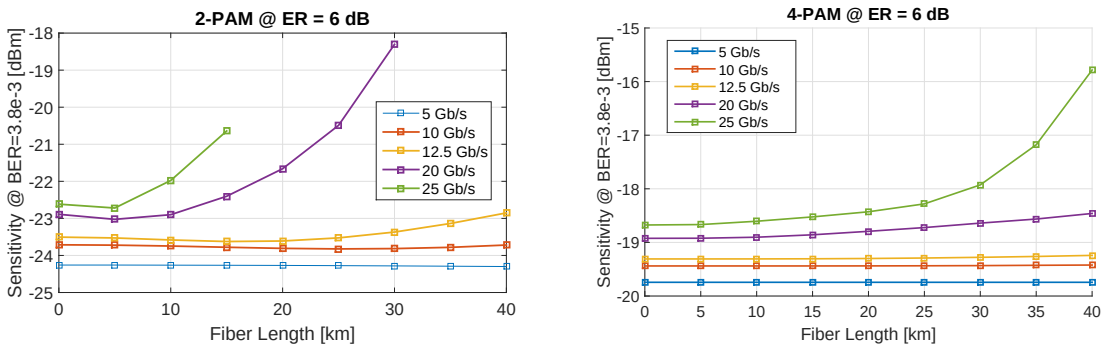

(a) 2-PAM modulation format.

(b) 4-PAM modulation format.

Figure 3.7: Variation of the sensitivity for different fiber lengths and bit-rate.

Observing the results above, is clear that 2-PAM is more sensitive to CD. The following equation 3.2 helps to comprehend this assumption and exposes the limit of the dispersion length L_D. The fiber length is dependent to the inverse of the squared baud-rate, B^2, upon the inverse of the squared λ_0, and upon the inverse of the absolute value of CD factor, $|D|$.

$$L_D = \frac{c}{2B^2\lambda_0^2\,|D|}, \tag{3.2}$$

According to this equation 3.2, the dispersion length decreases with higher bit-rates, as it was concluded by the simulation results in Figure 3.7.

For a better understanding of this phenomena, the following Figure 3.8, shows how the signal behaves with different dispersion values for 1 *km* of fiber. The bit-rate is 25 *Gb/s* and

the input power remains the same for all cases. The tests were done for both modulation formats, 2-PAM and 4-PAM.

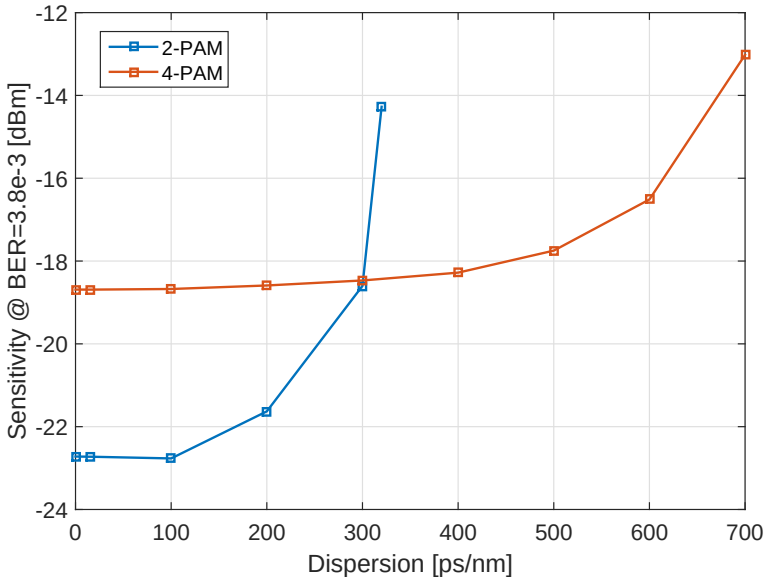

Figure 3.8: Sensitivity over the different accumulated dispersion.

Dispersion tolerance is hereby defined as the maximum total accumulated dispersion that the system is capable of receiving the signal.

3.2.3 Four channels system

At this point more channels were introduced. Instead of having only one, three more were placed. The system is almost the same but, since there are more channels, a multiplexer was necessary and also, a splitter to first combine the four output from the externally modulated signals and then equally divide into four photodetectors. A filter was placed to tune the desired wavelength to the respect PIN. Regarding the bit-rate, 25 Gb/s was the chosen value and the power of the laser emission is 1 mW.

The setup is in the following Figure 3.9.

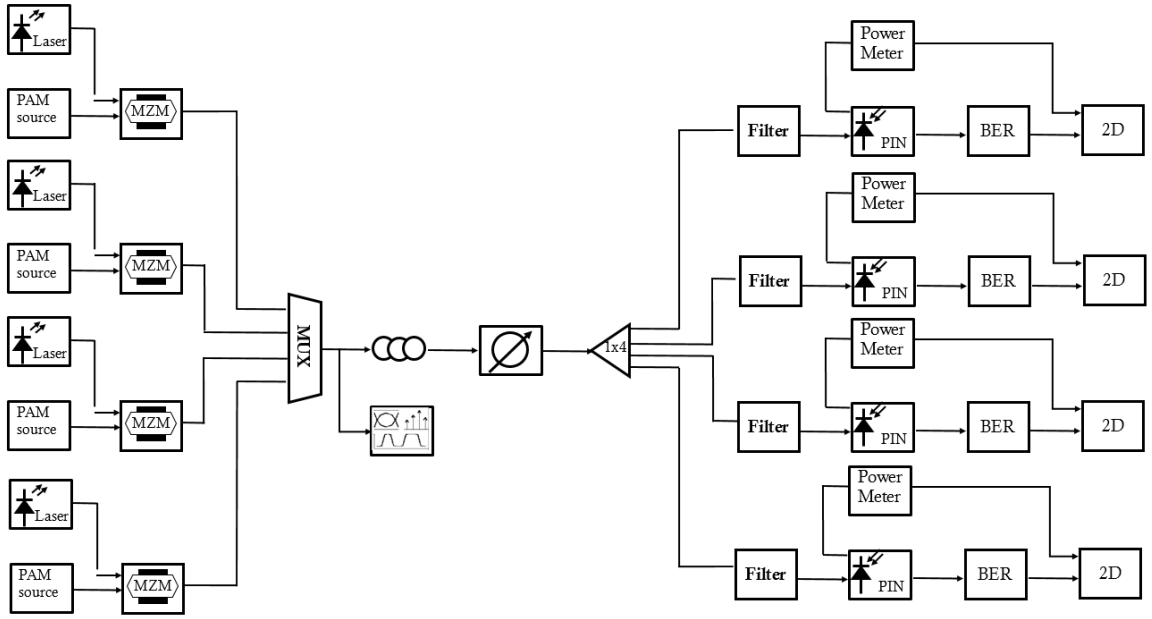

Figure 3.9: Setup to simulate the four channels system.

The system supports 4-PAM modulation and has four channels spaced by 100 *GHz* in C-band. The following table 3.1 shows the emission frequency of each laser.

Wavelength [nm]	**Frequency [THz]**
1530	195.94
1530.80	195.84
1531.29	195.74
1532.37	195.64

Table 3.1: Selected channels for the laser emission.

The optical spectrum of the transmitted signal in back-to-back way and without fiber is shown in Figure 3.10 below. It is noticeable the four channels where, the peaks correspond to the different wavelengths and consequently to the frequency. The channel spacing is another aspect that can be measured where 100 *GHz* was confirmed as specified in the settings of the setup. The peak power of each channel is -4.5 *dBm*.

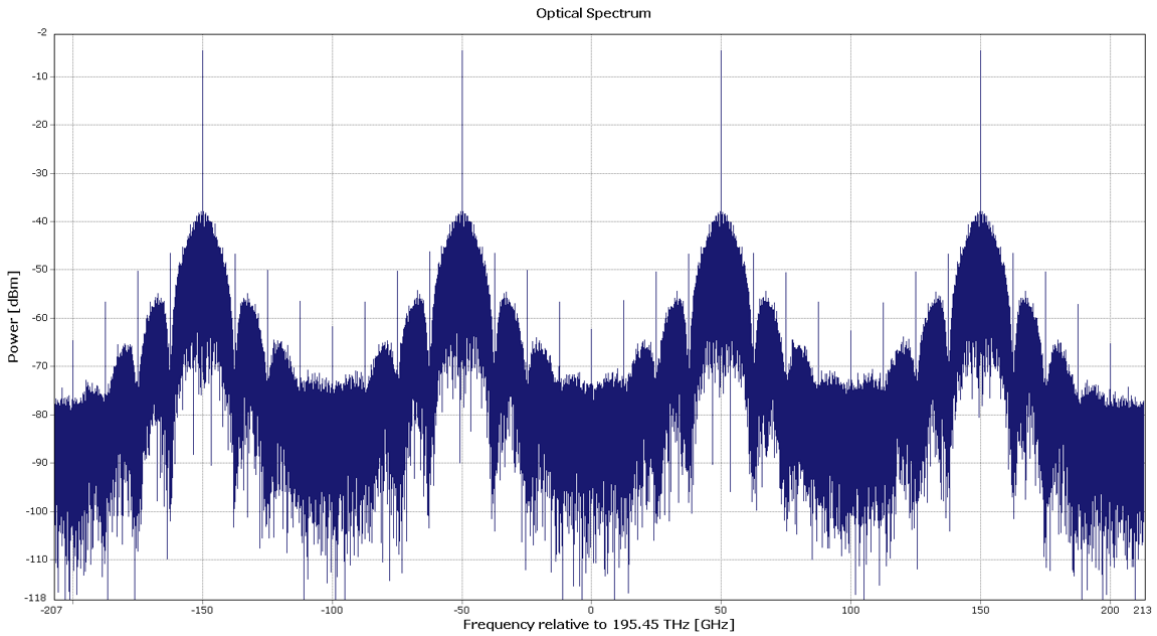

Figure 3.10: Optical spectrum of the 4-channel transmitted system.

The received optical spectrum result is displayed in Figure 3.11. After transmission, the combined signals are separated by a splitter, and each signal is detected individually. Once again, the channel spacing remains the same, 100 *GHz*, and the peaks correspond to the signal detected. The peak power of each channel is -10.6 *dBm*.

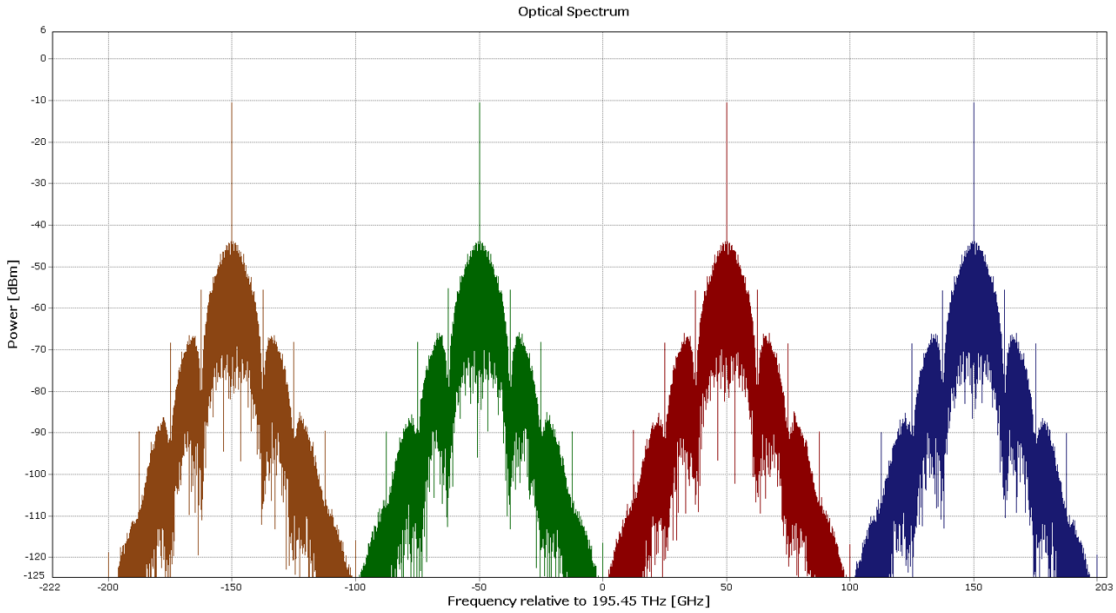

Figure 3.11: Optical spectrum of the 4-channel received signal.

The simulation has the purpose of testing the sensitivity for 10 *km*, 20 *km* and 40 *km*. This three fiber lengths were simulated over a bit-rate of 25 *Gb/s*. The following Figure 3.12 present the results for BER over the received power at the photodetector's input for each fiber length.

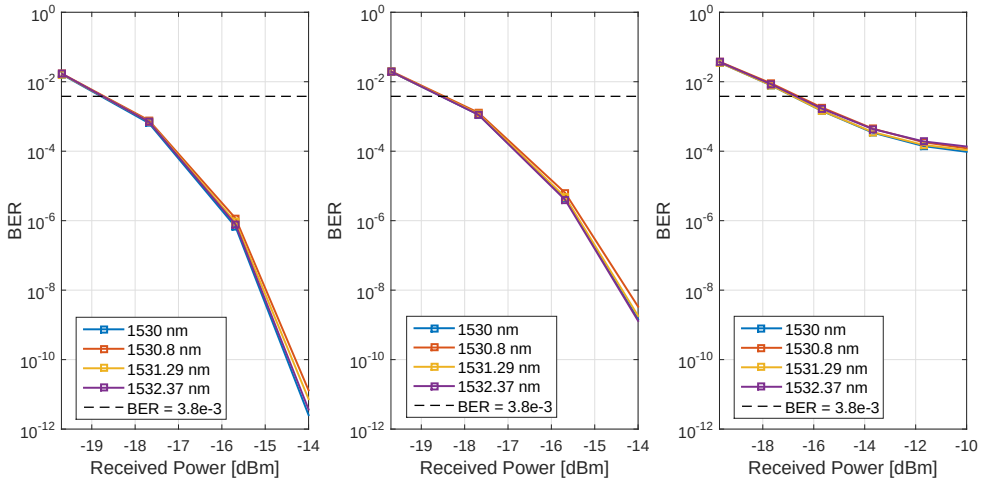

Figure 3.12: Sensitivity over received power for 4-PAM format with different fiber lengths: 10 *km*, 20 *km* and 40 *km*, respectively.

Observing the results above, it is clear that as the fiber length increases, the signal deteriorates more. The sensitivity at 3.8×10^{-3} is approximately -19 *dBm* for 10 and 20 *km*, but for 40 *km* is -17 *dBm*.

Chapter 4

Study of Photonic Integrated Components

This Chapter 4 presents the study and analysis of the optical components using a toolkit from VPIphotonics^{TM}. With this toolkit, called as VPItoolkit^{TM} PDK HHI, it was possible to test the performance and the behaviour of these components from the foundry Fraunhofer Heinrich Hertz Institute (FhG-HHI) giving the opportunity to for the first time make a simulation based on building blocks (BB)to then implement in PIC design.

Section 4.1 is dedicated to an overall description of the foundry and the toolkit. Right after, there are several sections with the setups and the results obtained from a simulation environment, which helped to understand how the components behave and their weaknesses.

4.1 Foundry and the Toolkit

FhG-HHI is a research institute with foundry capability based in Berlin, Germany, that was founded on 1st August 1927.

The competencies of the Fraunhofer HHI are in the areas of photonic networks, fiber optic sensor systems and video coding and transmission. The research works of the institute are consistently oriented towards its fields of expertise and offer attractive solutions for market and development demands of the present and the future [29].

This company is one of the three most famous chip manufacturers that provides access to InP-based generic foundry processes. Besides that, it is integrated into a European consortium called JePPIX. The members of the consortium, allow the users to apply for MPW, where wafers are shared among users and so also the costs, reducing the prototyping prices of the

optical systems. Moreover, the foundries provide to the users the Photonic Design Kits (PDK), that contains basic buildings e.g. couplers and lasers that were already tested and fabricated leading to a "first-time-right" design [3].

VPItoolkit PDK HHI is a plug-in available developed by VPIphotonics^{TM} in straight collaboration with FhG-HHI. With this toolkit, the user is able to perform component and system level simulation of the monolithic PIC and export the setup to the mask level. The tool enables the user to choose certain types of building blocks like waveguides, lasers, junctions, photodiodes, optical amplifiers, couplers. After the design, it is possible to fabricate it at the FhG-HHI foundry [30].

Another feature about this toolkit is the possibility of exportation to the PhoeniX OptoDesigner software. Once the design of the circuit is done there is an option that allows to export it, and the mask layout will be generated in the OptoDesigner environment. It fits the design in the package, adds proper electrical wire routeing, performs a design rule check (DRC) verification, and finally exports the GDS mask (the industry standard format) for optical chip fabrication.

It is important to note that this toolkit is still in trial period and some functionalities are not totally working, for example is the translation from the setup on VPIphotonics^{TM} to the mask layout, that is why in Chapter 5 the implementation of the layout is presented using OptoDesigner software.

The work performed using this VPItoolkit PDK HHI on testing the building blocks's performance is presented in the following sections. It is important to refer that this toolkit does not provide access to the layout contents of the building blocks which remains proprietary information of the foundry. Concerning to the values used for the simulations/tests, those were chosen according to the foundry's Design Manual suggestions. Besides that, since this was also a system's test and this was the first trial version available in the market, the defects from this toolkit were also reported to the foundry, helping them to improve its quality.

4.2 Waveguides

The foundry provides four types of waveguides: Straight, Tapered, Arc, and S-bend. According to their rib height in the substrate, the foundry characterizes the passive waveguides in three different geometries: the E200 waveguide with a height of 200 nm, the E600 waveguide with a height of 600 nm, and the E1700 waveguide with 1700 nm of height. The following Table 4.1 give us an overview of the available waveguides and their available geometries.

Straight	Tapered	Arc	S bend
E200	E200	E600	E600
E600	E600	E1700	E1700
E1700	E1700		

Table 4.1: Passive waveguides available in FhG-HHI foundry.

4.2.1 Straight Waveguides

The straight waveguide block contains one input and one output. This BB gives the permission to change just two physical parameters: the length and the width. For this building block, the power loss was tested as a function of length for the different available geometries.

4.2.1.1 Setup and Results

The setup that is in Figure 4.1 is the one that was used to test the power losses on this kind of waveguide.

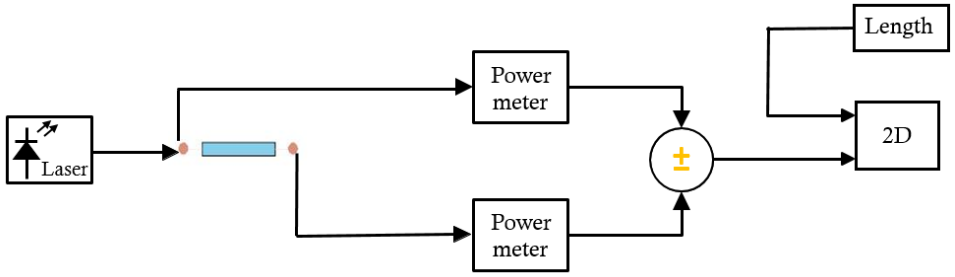

Figure 4.1: Simulation environment to measure the power loss as a function of the length for the three different geometries: E200, E600 and E1700.

The first block is an ideal laser producing a continuous wave (CW) optical signal. It is connected to the desired passive waveguide. This waveguide has an intern sweep in the length parameter from 0 to 1 cm with an incrementation of 100 μm and a fixed width of 2 μm that is the recommended value from the foundry for single mode guiding. After that, two power meters were placed. One at the input of the waveguide and another at the output. These power meters measure the power at the input and output of the block, giving us the final power loss in dBm. These values will be shown on the 2D graph, where the X-axis concerns the length, and the Y-axis contains the losses at each length.

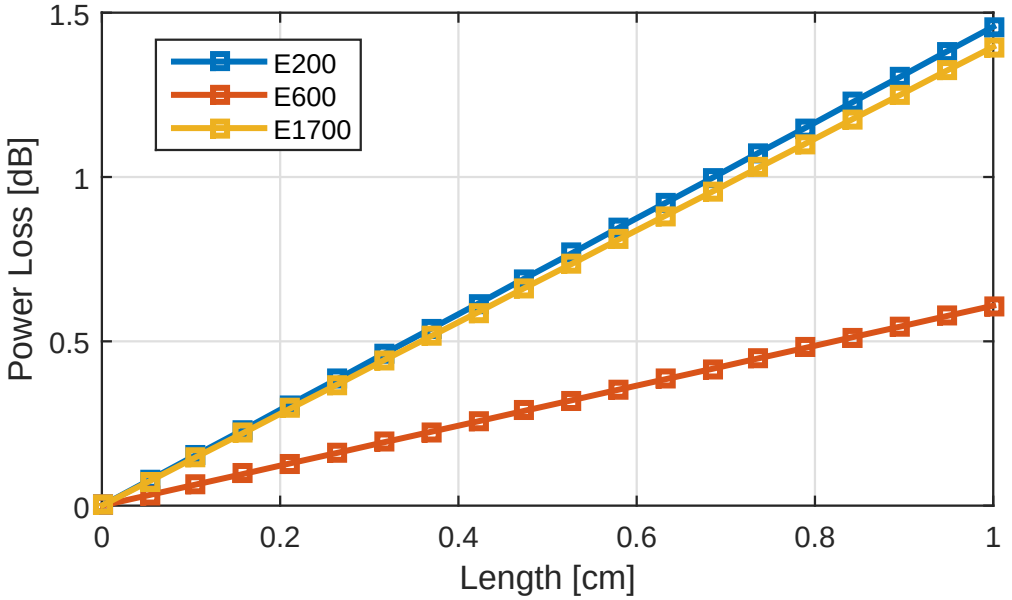

Figure 4.2: Power loss as a function of length for different waveguide's geometries (E200, E600 and E1700).

Figure 4.2 shows the difference of power loss between the three geometries. The E200 has 1.5 *dB/cm* of loss, the E1700 has 1.4 *dB/cm* and the E600 has 0.61 *dB/cm*. The E600 is the waveguide that owns fewer propagation losses, but these results do not correspond to what was expected. According to the Design Manual [31], the one that holds lower power loss is the E1700. Due to he higher etching, this waveguide has more contrast between the core and the cladding which results in a more confined light and subsequently in lower losses.

4.2.2 Tapered Waveguides

A tapered waveguide block owns one input and one output. The length, the input waveguide width and the output waveguide width are the three physical parameters that one can change. For this block, the propagation loss was measured as a function of length for the different geometries available.

4.2.2.1 Setup and Results

Here, in Figure 4.3 the setup to test the power loss of the tapered waveguides is presented for the different geometries: E200, E600 and E1700 and for the different output waveguide widths.

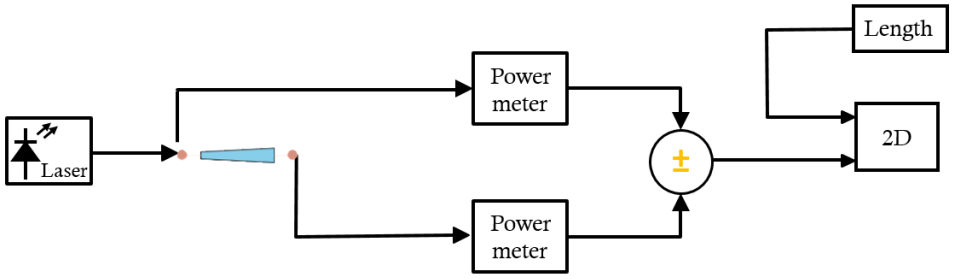

Figure 4.3: Simulation environment to measure the power loss as a function of the length for the three different geometries: E200, E600 and E1700, with different output widths

This configuration (Figure 4.3) is similar to the previous one, in Figure 4.1, but instead of a straight waveguide, there is a tapered one.

The results are in Figure 4.4, where for each possible geometry the power loss is measured for two different output widths: 2.5 μm and 3 μm. The input waveguide width used was 2 μm.

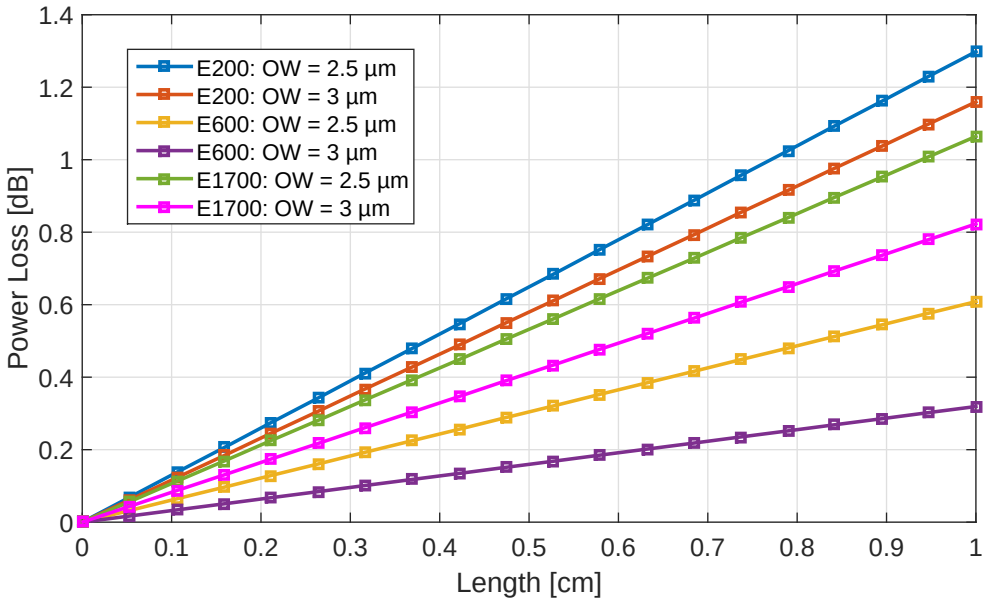

Figure 4.4: Power loss as a function of length for the three different waveguides geometries (E200, E600 and E1700) and for various output widths.

In the legend of Figure 4.4, the "OW" correspond to the established output width. As expected, the E200 waveguide is the one that has more propagation loss for both output width. Another conclusion is that, for an increase of the output width, it will lead to a

decrease of power loss.

With this simulation, the E600 is the one that has less power loss, again. These results were not the expected ones, which drives us to conclude that this particular waveguide was not well modelled in this version of the toolkit.

4.2.3 Arc Waveguides

The arc waveguide is a curved bend that has one optical input and one optical output. The building block is only available in the E600 and E1700 geometries. It contains three physical parameters that are apt to change: the radius, the angle and the width of the waveguide.

4.2.3.1 Setup and Results

Once again the setup used is similar to the previous ones. In Figure 4.5 shows the setup to test the power loss but in this case is regard to the angle. It was tested for different waveguide radius with a fixed width of 2 μm suggested by the Design Manual.

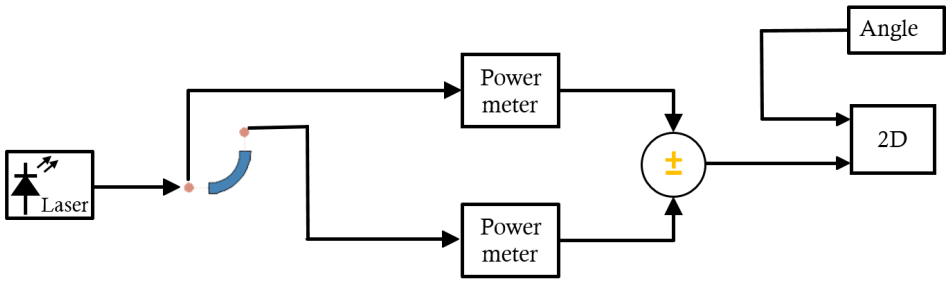

Figure 4.5: Simulation environment to measure the power loss as a function of the angle for the two different geometries: E600 and E1700.

The results of this simulation are in the following Figure 4.6. The "R" letter presented in the legend refers to the chosen radius.

In Figure 4.6 it can be seen that for the E600 waveguide, for 400 μm the power loss for 90° is 0.04 dB and for 480 μm the power loss for 90° is 0.05 dB. In case of the E1700 waveguide, there is 0.03 dB of loss for 150 μm and 0.05 dB of loss for a radius of 250 μm. So, for higher radius, the power loss will be higher too, as expected as the radius is increased, the arc waveguide will be higher and will also increase the losses due to reflections.

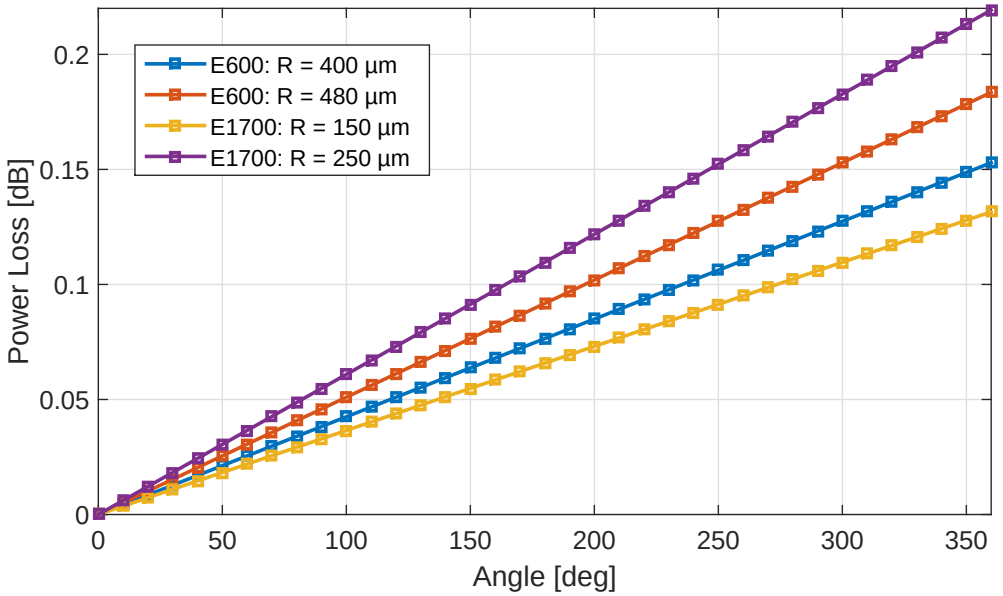

Figure 4.6: Power loss as a function of angle for different waveguides geometries (E600 and E1700) and different radius.

4.2.4 S Waveguides

The last waveguide to be present is a S bend. This block is available in two geometries: E600 and E1700. It is possible to modify three parameters: the length, the width and the height.

4.2.4.1 Setup and Results

The setup is shown in Figure 4.7 where the aim of it is to measure the power loss as a function of the length for the different geometries and various widths. The height was not changed, and it was set to 10 μm because no changes were noticed with various values.

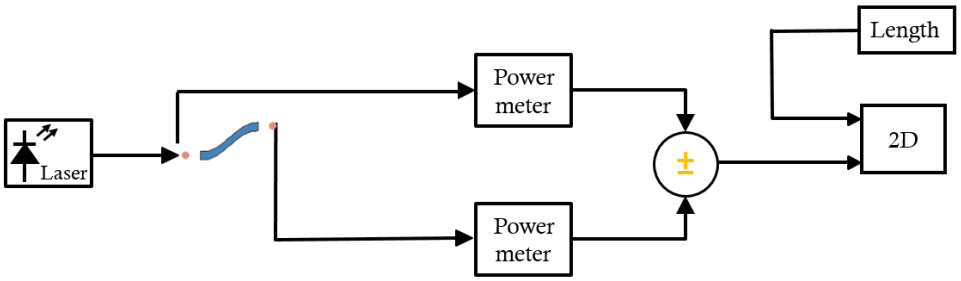

Figure 4.7: Simulation environment to measure the power loss as a function of the length for the two different geometries: E600 and E1700.

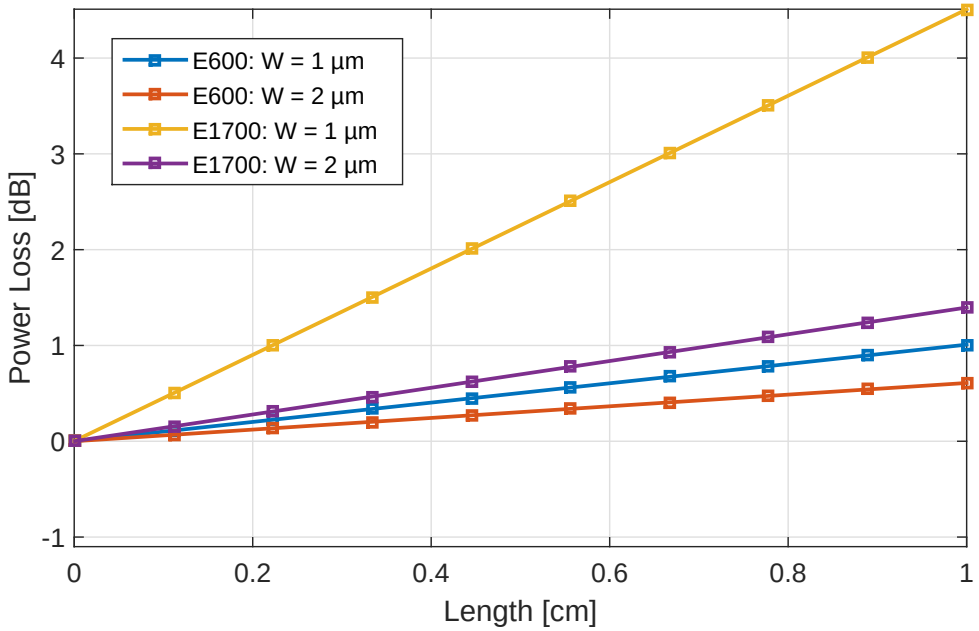

Figure 4.8: Power loss as a function of length for different waveguides geometries and various widths.

Concerning to the Figure 4.8, there is a significant difference between the yellow line (corresponding to E1700 with 1 μm of width), to the others. At 1 *cm*, in the yellow case, the power loss is around 4.5 *dB*. The other ones are around 1 *dB*. This difference should not be expected and it was a problem reported to the toolkit provider.

4.3 Directional Coupler

The directional coupler is a block that splits the light into two fractions. The ratio between these fractions depends on to the coupling length. This BB is only available in E600 geometry and it has four ports: two optical inputs and two optical outputs. The length of the coupler is the only physical parameter that can be changed.

4.3.1 Setup and Results

The simulation environment is in Figure 4.9. It starts with a CW block, an ideal laser with 1 mW of power connected to the coupler. The directional coupler has an internal sweep in coupler length from 0 to 600 μm and right after one can observe two power meters allowing the calculation of the output power at the difference outputs. The graph is the 2D block, where it introduces the length in the X-axis and the output power in the Y-axis.

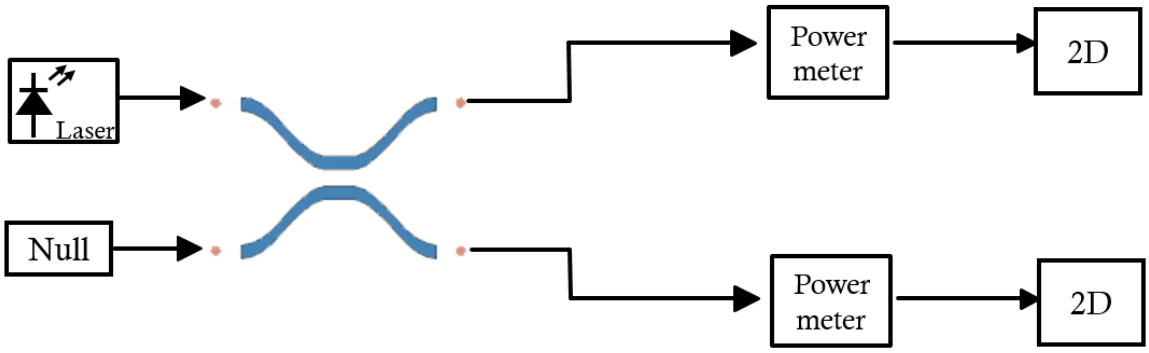

Figure 4.9: Simulation environment to test the output power in the provided directional coupler.

In Figure 4.10 the output power of the directional coupler is stated for different coupler lengths. To achieve these results, first, the laser was placed in the upper arm (1st arm), and the simulation was done. After that, the laser changed to the bottom arm (2nd arm), and the results were registered again.

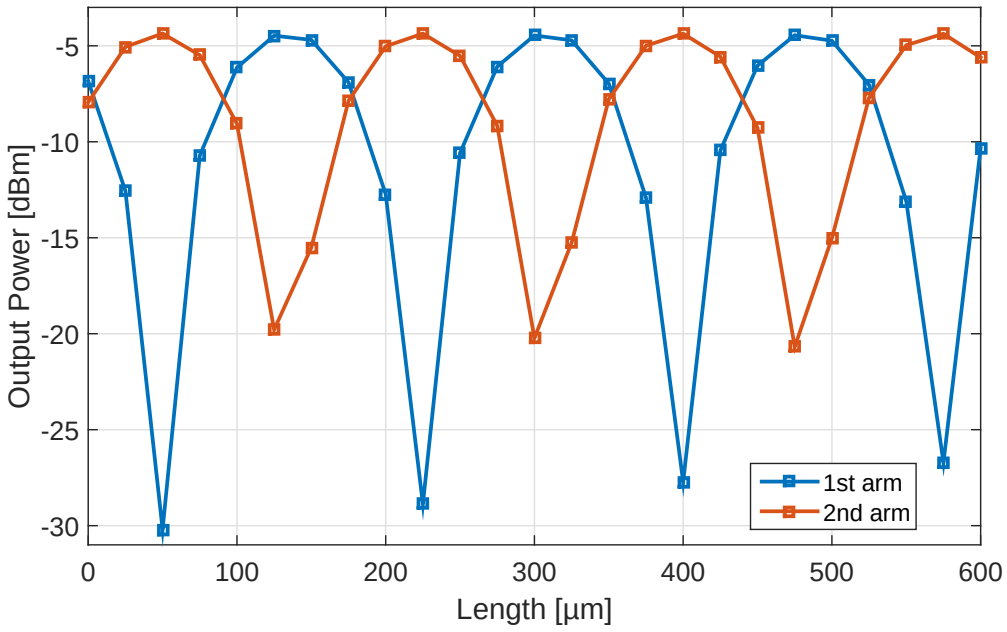

Figure 4.10: Output power of the directional coupler in the two arms with different lengths.

The maximum output power in the 1^{st} arm, occurs at 475 μm of length with -0.7 *dBm*. On the other hand, for the 2^{nd} arm the maximum occurs at 50 μm with -0.6 *dBm*. Another characteristic is the insertion loss, that is 0.6 *dB*. The previous values already take into account the 3 *dB* of power loss from the coupler because of its divided signal power. This value is in agreement with de Design Manual.

The power coupling was also tested according for different coupler lengths. With this information it is then possible to design all types of couplers with power balance ratios between outputs, in the particular case of 50% ratio the 90.8 μm should be the chosen length.

4.3.2 1x2 and 2x2 Multi-Mode Interference

A Multi-Mode Interference (MMI) coupler is the component chosen to split and combines signals. The foundry has two geometries available for this element: E600 and E1700. It has one available physical parameter to modify, the coupling length.

4.3.3 Setup and Results

These components were tested in order to characterise their output power. The setup is represented in Figure 4.11 where the MMI was replaced to the desired one.

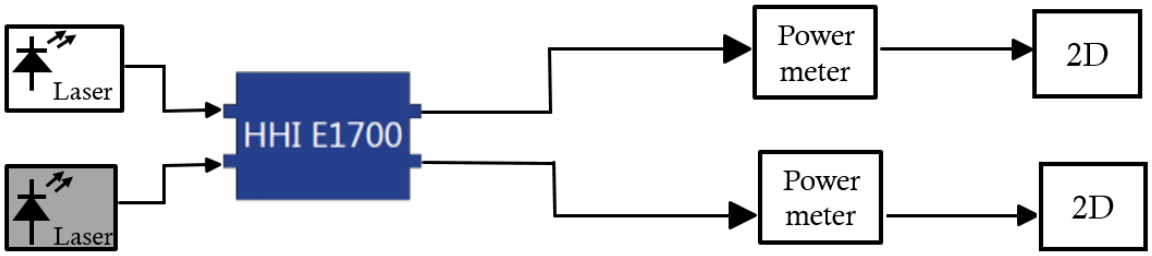

Figure 4.11: Setup used to characterize the behaviour of MMI.

Regarding the 1x2 E1700, the output power in the first arm is about -4.1 *dBm* and in the second arm in -3.9 *dBm*. In the 1x2 E600, the output power in the first arm is about -3.9 *dBm* and in the second arm in -4.1 *dBm*.

In conclusion, the power in each arm is around 4 *dBm*, and since they split the input signal in half (half of the power is going to each output: 3 *dB*), the insertion loss is around 1 *dB* that is in concordance with the specifications.

Concerning the 2x2 MMI, two lasers were connected to the inputs of the BB. The main goal is to see the output power of each arm. So, for each simulation run, one laser was disconnected.

When the upper laser is connected, the output power from the first arm is -3.8 *dBm* while the second one is -4.3 *dBm*. Then, when the active laser is changed to the bottom one, the output power in the first arm is -4.3 *dBm* and the second one is -3.8 *dBm*. These results are the same using E600 or E1700 geometry.

4.4 Thermo-Optic Phase Shifter

The thermo-optic phase shifter is a phase modulator based on the thermo-optic effect. Through the length and the current in the heater, this modulator is capable of changing the phase of the input signal. The modulator consists of a 2 μm-wide straight waveguide covered by a silicon nitride isolation layer and also a thin metal layer as the heater element. The foundry provides three different geometries for the phase shifter: E200, E600, and E1700. In the case of the E200 heater-based phase modulator, the heater is physically placed on top of the waveguide. On the other hand, the E600 and E1700 modulators keep the heater at about 3 μm next to the waveguide. The phase shifter present only one physical parameter that can be modified: its length, nevertheless it is also possible to control the current that is externally

input in the heater.

4.4.1 Setups and Results

The setup on Figure 4.12 simulates a Mach-Zehnder structure. There is a block that models a DFB laser producing a continuous wave (CW) optical signal whose power was set to 1 mW and the wavelength (λ) is equal to 1550 nm. The light generated goes through the 1×2 MMI E1700 where the signal is split onto two different waveguides. In the upper arm, the shifter has a fixed length and the current is changing. However, in the bottom arm there is also a phase shifter, but in this case, the current is 0 mA. After this, there are again two waveguides and a 2×1 MMI E1700 to join the signal. With this setup, one can see the different shifts between the two arms. When the upper and lower arms are in phase, it is possible to observe that there is the maximum output power but if they are in opposite phase, the output power will be at its minimum. This was the main setup used for the three geometries (E200, E600 and E1700). To test each of them, the desired phase shifter was replaced.

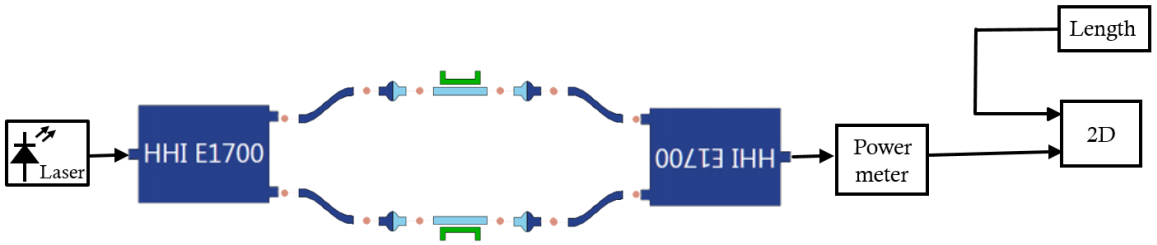

Figure 4.12: Power as a function of current of the phase modulator for different heater lengths.

The results obtained for the E200 phase shifter are presented in Figure 4.13. It was considered five different heater lengths: 200 μm, 250 μm, 300 μm, 350 μm and 400 μm.

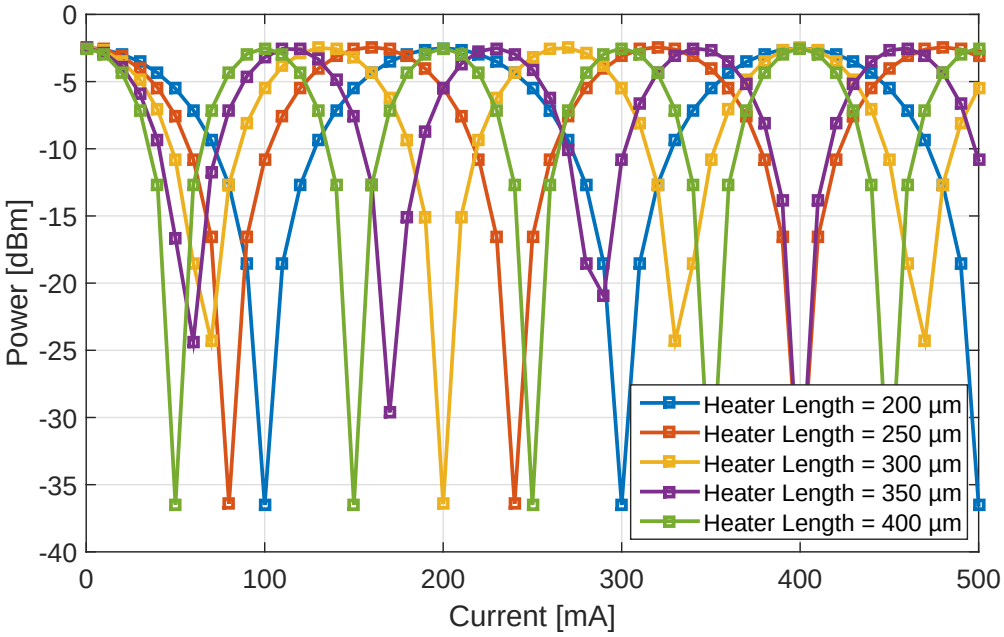

Figure 4.13: Power as a function of current of the phase modulator for different heater lengths using E200 thermo-optic phase shifter.

The behaviour of the E200 phase modulator with different heater lengths is represented in Figure 4.13. As expected, the curves are dependent on the injected current. The minimum output power for each heater lengths gives us the necessary value of current to obtain a phase shift of 180°. It means that, for example, for 200 μm of heater length, if the user wants a π phase shift it is needed to inject 100 mA, 300 mA or 500 mA, because the $I_\pi \times L$ of this component is $20mA \times 1mm$. The same conclusions can be taken for the other heater lengths.

The following Figure 4.14 present the results obtained for the E600 and E1700 phase shifter, considering five different heater lengths. These two geometries have the same behaviour as it says the Design Manual [31] as was verified by those simulations.

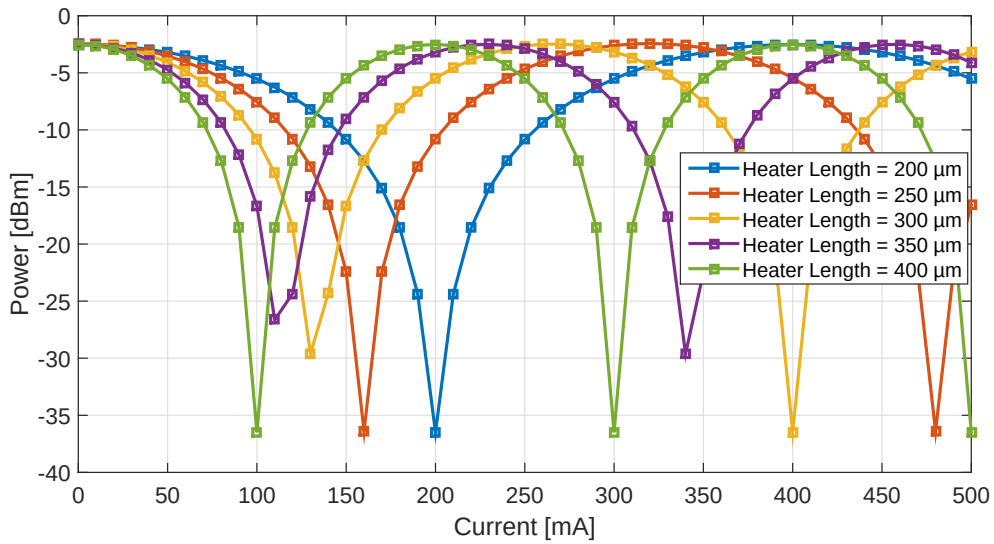

Figure 4.14: Power as a function of current of the phase modulator for different heater lengths using E600/E1700 thermo-optic phase shifter.

Once again, the power is dependent of the current injected and also of the heater length. In this case, if a 200 μm heater length is used, for a phase shift of 180° it is necessary to inject 200 mA because, in case of E600/E700, the $I_\pi \times L$ of this component is $40mA \times 1mm$. So, the E600/E1700 phase modulator needs twice more current to have a change of 180° comparing to E200.

The conclusion taken from the three phase shifters is that with an increase of the heater length, leads to a decrease of the injection current. This is not necessarily the best option considering the length of the component that will conduct to higher losses and consequently to a bigger space consumption in designing the PICs.

4.5 Semiconductor Optical Amplifier

The SOA available by the foundry is a component based in a MQW (multi-quantum-well) structure. This block includes two butt-joints for coupling between active and passive (E200) waveguides.

4.5.1 Setup and Results

In Figure 4.15, the main setup used to study the behaviour of the SOA can be seen. There is an input ideal continuous wave with an emission frequency at 1550 nm and a power of 1

mW that is sent through the amplifier block. The length of a SOA is the only parameter that can be changed. A DC current source was introduced where current is injected through the SOA. A power meter is placed at the input and at the output of the amplifier to measure the gain of the amplifier that is going to be displayed in the 2D plot.

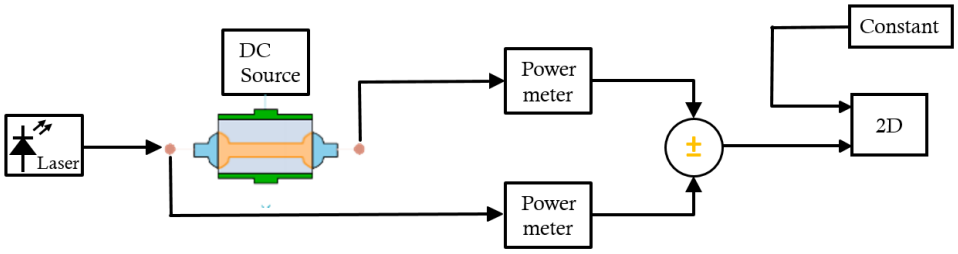

Figure 4.15: Simulation environment to characterize the SOA.

To characterise a SOA three figures of merit were chosen: the gain, the gain bandwidth, and the saturation output power. The gain is the factor by which the input signal is amplified, it varies with length and current. The gain bandwidth is the optical range of the spectrum where the amplification occurs. Finally, the saturation output power that the SOA can provide, with a value dependant on the length and current injected.

Concerning these key parameters referred before, the following Figures 4.16, 4.17, 4.18, shows the behaviour of this amplifier in this toolkit.

The first test has the goal of observing the dependence of the gain with the input power. The length of the SOA is fixed for 300 μm and the current injection varies between [0, 10, 25, 50, 100, 150, 200] mA. A sweep on the laser power was introduced, going from -32 dBm to 20 dBm.

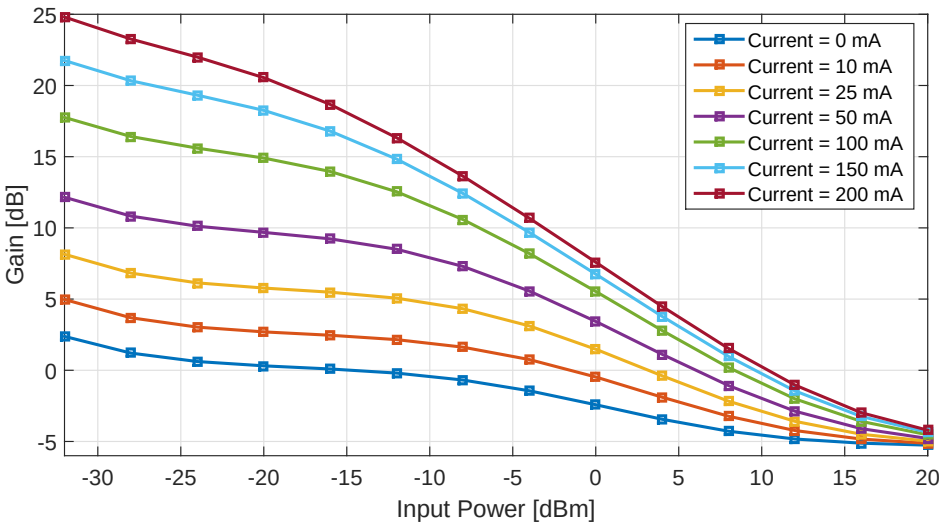

Figure 4.16: Variation of the gain with the input power, assuming different injected currents.

Figure 4.16 shows the results of the SOA model. The results give the variation of amplification (gain) with an increase in the input signal power for different values of bias current (mA). Firstly, looking at the results in Figure 4.16, it is evident that with more current leads to more gain. With 200 mA is possible to have a maximum gain of 25 dB but, for 50 mA of injection current, the gain will be almost half of the previous one. A higher gain results in a higher output optical signal. However, the gain of an optical amplifier is not unlimited. At a certain point, is observed that the SOA starts to saturate and it drops significantly. This fact happens when the amplifier is operating out of the linear regime [32]. The saturation point results from 3 dB of reduction of gain. At this point, adding the gain and the input power, it will give us the exact output saturation point. For example, for 50 mA of injection current and an input power of -20 dBm, the gain is about 13 dB.

Another aspect is that the amplifiers should have a minimum input power since the amplifier cannot achieve gain with too low input powers. Unfortunately, is not happening the expected behaviour in this model since the gain keeps increasing even with such low input powers.

The following test is regarding the dependence of the gain with the length of the device. The input power of the laser is set to -20 dBm. The length of the building block is changing from the minimum active length provided from the foundry, 50 μm, till 500 μm. and the injection current vary between [0, 10, 25, 50, 100, 150, 200] mA. The Figure 4.17 shows the results of the gain over the length of SOA for different injection currents.

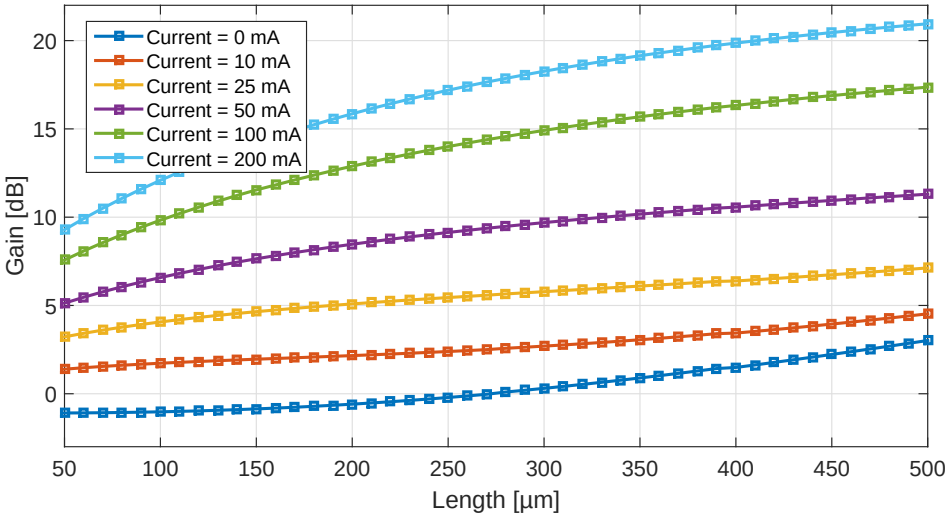

Figure 4.17: Gain dependence with the length, assuming different injected currents.

The results from the Figure 4.17 reveals that increasing the length of the SOA, the gain will also increase. The maximum gain is achieved when there is an injection current of 200 mA with a length of 500 μm.

The following test presents the dependence of the gain with the wavelength. The input power of the laser is set to -20 dBm and the length of the amplifier is fixed for 100 μm. Once again, the injection current vary between [0, 10, 25, 50, 100, 150, 200] mA. These simulations were done to check if the gain varies with the wavelength.

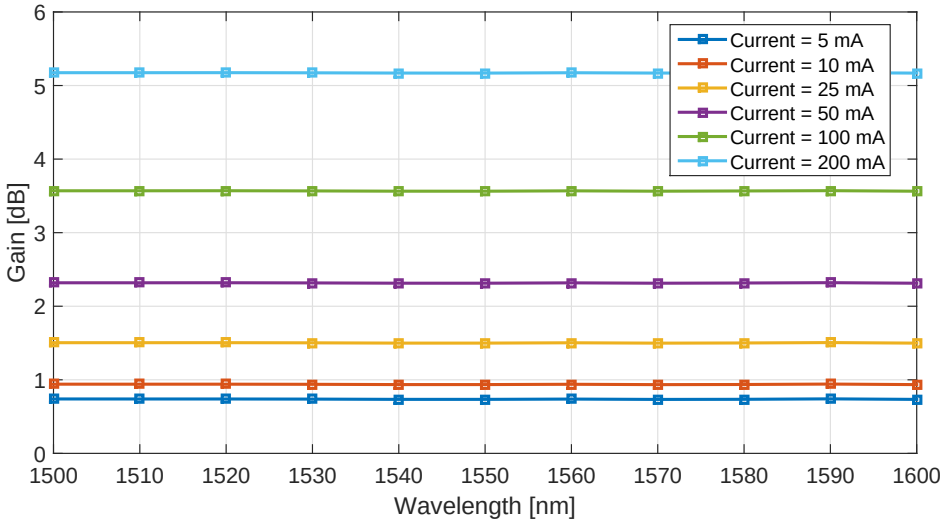

Figure 4.18: Gain as a function the wavelength for different currents.

An optical amplifier operates in a certain range of signal wavelengths. This range depends on the type of the amplifier. Usually, a SOA operates between 1280 *nm* to 1650 *nm*. In this range, the gain will be bigger. The dependence of the gain with the wavelength has an almost parabolic shape like it is represented in Figure 2.6 from Chapter 2.

The SOA from this toolkit does not exhibit the performance that was supposed to. The conclusion is that SOA is not entirely modelled and these factors are not being taken into account. The indication from the toolkit provider is that the component is optimized for 1550 *nm* and the work for the other bands of operation is under development.

4.6 Preamplifier Photodiode

At this moment, it was studied the pre-amplification of a photodiode. It is important to refer that the analysis of this photodiode by itself was performed in [33]. The foundry provides two different photodiode but the one used was the photodiode that has 3 *dB* of bandwidth at 20 *GHz*, and it is placed on the top of an E200 waveguide. The main focus on studying this block was to check its performance in sensitivity for a preamplified photodiode that consists of a SOA before the photodetector. Due to the higher gain given by the SOA, the system will have increased sensitivity.

4.6.1 Setup and Results

The setup used is presented in the following Figure 4.19. As it was said, the main target here is to test the sensitivity of this preamplified photodiode, for different fiber lengths. The setup starts with a module that simulates an externally modulated laser NRZ-OOK (on-off keying transmitter) that has a CW laser with a frequency emission of 1550 *nm* and an average power of -10 *dBm*. Then, it is connected to an optical fiber that has four possible lengths: back-to-back (0 km), 10 *km*, 20 *km* and 40 *km*. The value of the dispersion was set to 16 $ps/(nm \times km)$. After that, it appears an attenuator that produces an increasing attenuation of 30 *dB* starting from 0 *dB* with an increment of 1 *dB*.

The SOA is placed before the photodetector and it has 200 μm of length and 200 *mA* of injection current. The power meter is capable of measure the input power of the preamplified photodetector in *dBm*. The following module is used to determine the bit error ratio (BER). This approach estimates the number of bits with errors over the total number of bits. To do so, a bit-rate of 10 *Gb/s* was chosen.

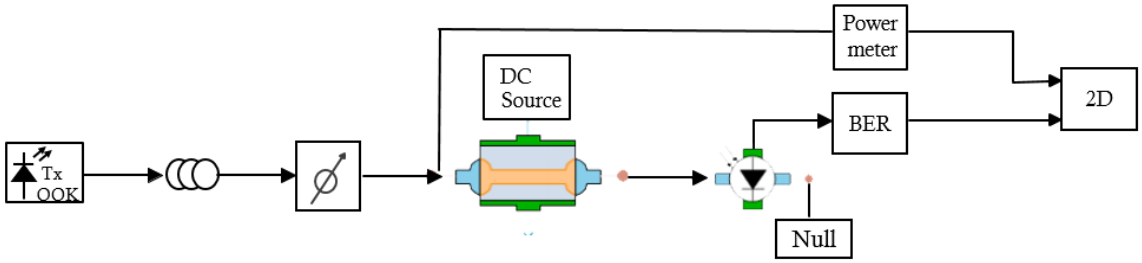

Figure 4.19: Simulation environment to test the pre-amplifier photodetector.

Observing the results presented in Figure 4.20, the BER over the received power in the photodetector is shown. Four different curves, from four different fiber lengths, are presented. The other line is the threshold BER which correspond to 3.8×10^{-3}.

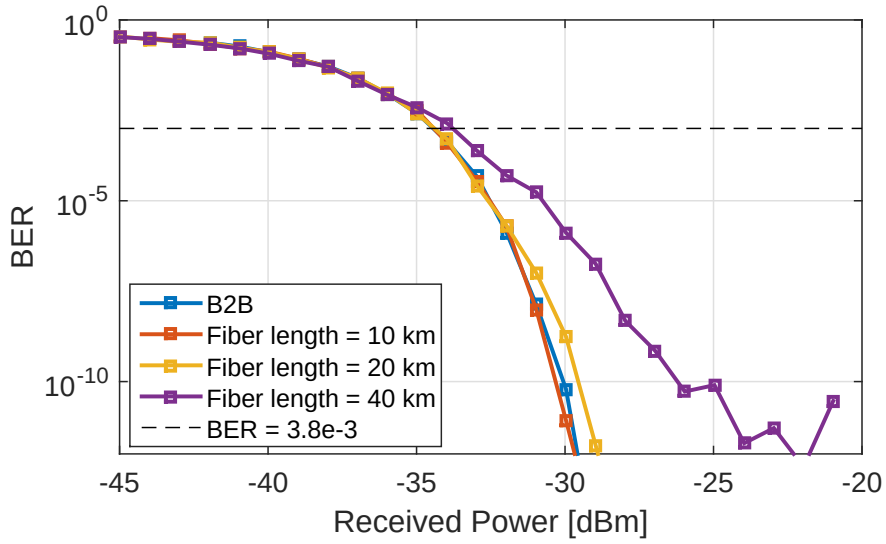

Figure 4.20: Received power for the pre-amplified photodetector using 10 *Gb/s* of bit-rate.

It is noticeable that for a BER of 3.8×10^{-3}, the received power is -35.8 *dBm* that is almost the same for 0 *km*, 10 *km*, and 20 *km*. With 40 *km* of fiber length there is a small difference of the received power at the same BER value, but not significant: -35 *dBm*. It means that for 0, 10 and 20 *km* the attenuation overlaps the dispersion effect, but in the case of 40 *km*, the dispersion starts to have a most notable appearance.

Using the formula 3.2 presented in Chapter 3, the limit imposed by the dispersion considering NRZ-OOK modulation is 39 *km*. So, the dispersion effect at 40 *km* is presumed as it is exposed in the simulation.

In order to compare the performance of using a pre-amplifier photodiode instead of using just the photodiode is relevant to remember that, for 200 μm of length and 200 *mA* of injection current, the gain is around 15 *dB*, as presented in Figure 4.17. The sensitivity of the photodetector without pre-amplification was studied in [33]. There, the received power for 10 *km* was -20.4 *dBm*. It can be concluded that adding the amplifier was possible to push the sensitivity 15 *dB* more, coming up to the -35 *dBm*.

The test for 25 *Gb/s* of bit-rate was also performed. In this case, the received power in B2B and for a BER of 3.8×10^{-3} is -33.7 *dBm*. For 10 *km* the received power is -32.9 *dBm*. After 10 *km* the photodetector is not able to receive the signal.

One can conclude that this pre-amplifier photodiode is a possible solution for a system that needs higher sensitivity as it is often required in PON architectures.

Chapter 5

Development of the Transceiver Architecture

After an extensive study of the building blocks from the FhG-HHI foundry performed in the last chapter, the chosen transceiver architecture is introduced in this one. Furthermore, all the steps to design and simulate this architecture are presented in this chapter.

The Chapter begins with a block diagram in which the main sections of the architecture are represented by blocks revealing the relationships between them (Section 5.1). After that, the development of the overall structure is described, starting with the two AWGs that will perform as Multiplexer/Demultiplexer in section 5.2.

Then, in Section 5.3, the layout implementation of the building blocks designed with the OptoDesigner software is presented. This section is divided into two subdivisions for a clear understanding of the design. The transmission block is shown first (Subsection 5.3.1), where the principal and the steps for the design are revealed. Afterwards, in Subsection 5.3.2, the reception block is presented where the same explanation as before is done.

The Chapter ends with the final mask layout.

5.1 Transceiver Architecture

There are several candidate wavelengths allocation plans for the NG-EPON, under discussion. For this work in particular, the C plan [5] was chosen where the wavelength band is 10 nm wide in both directions. The downstream direction is allocated between 1595 *nm* and 1605 *nm* which is related to the L-band of the spectrum, while the upstream band is placed between 1530 *nm* to 1540 *nm* from the C-band of the spectrum.

Upstream direction		Downstream direction	
Wavelength [nm]	Frequency [THz]	Wavelength [nm]	Frequency [THz]
1530	195.94	1595	187.95
1530.80	195.84	1595.91	187.85
1531.29	195.74	1596.76	187.75
1532.37	195.64	1597.62	187.65

Table 5.1: Selected channels for downstream and upstream directions.

Hence the selected channels, to design the transceiver are in Table 5.1. It consists of four channels in both directions, upstream and downstream. The channels are spaced by 100 *GHz*, which is a feature from a WDM system.

Through some tests done on lasers from FhG-HHI, it was concluded that this building block only transmit on the range of [1520, 1570] nm [33]. So, regarding the plan presented before, this laser can transmit just on upstream direction. Because of this factor, the architecture that will be presented is working as a transceiver but just in the ONU side. Moreover, this transceiver should also support the 4-PAM modulation format.

Before starting to design a PIC, it is crucial to have an overall idea of the architecture to be implemented. In the following Figure 5.1, the complete structure of the transceiver is given using block diagrams. This diagram exposes the relationship between the blocks, so one can understand how this architecture works as a system.

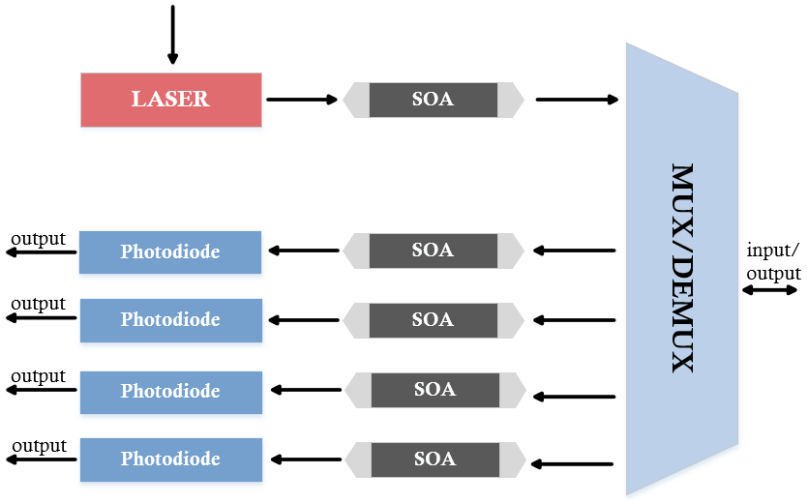

Figure 5.1: Block diagram of the transceiver.

The block diagram is divided into three main sections: the transmission blocks, the Multiplexer/Demultiplexer and the receiver blocks.

In a brief explanation, in the transmission side there is a DFB laser capable of tuning to the desired wavelength and goes through an SOA which amplifies the signal power. The signal combines in a Multiplexer, whose functionality will be described shortly. For the reception side, the signal comes from the input/output interface (fiber entering in the chip), is separated using the Demultiplexer, and it is received by the preamplified photodetectors. The receptors are composed by four SOAs that amplifies the signal and four photodetectors to detect it and convert it into electrical signals.

5.2 Design and Simulation of the Multiplexer / Demultiplexer

The development of the design and simulation of the Multiplexer / Demultiplexer will take place in this section. This block, as it was mentioned, it will be used as a multiplexer or as a demultiplexer. So, when it is working in the receive mode, the block will act as a demultiplexer, dividing the four channels in four paths to the respective photodetector.

5.2.1 Aspic^{TM} Simulator

For the development of the Multiplexer / Demultiplexer, an user interface called Aspic^{TM} was used, an acronym for Advanced Simulator for Photonic Integrated Circuits. Aspic^{TM} is a simulator for the analysis, modelling and design of photonics integrated circuits. It allows constructing every circuit starting from the components available in its library, without any restriction in dimensions and complexity [34]. This software contains several libraries from different foundries where the PDK from FhG-HHI is one of them.

5.2.2 AWGs in Aspic^{TM}

This section explains all the steps done to achieve the desired Multiplexer / Demultiplexer using Aspic^{TM} simulator with the supported PDK from FhG-HHI. For that, two different AWGs that work together as a system were designed. This system is composed of one AWG 1x2 and an AWG 1x4 connected with each other. To build these AWGs some aspects were taken into account. Figure 5.2 depicts these parameters to consider when the design is being done.

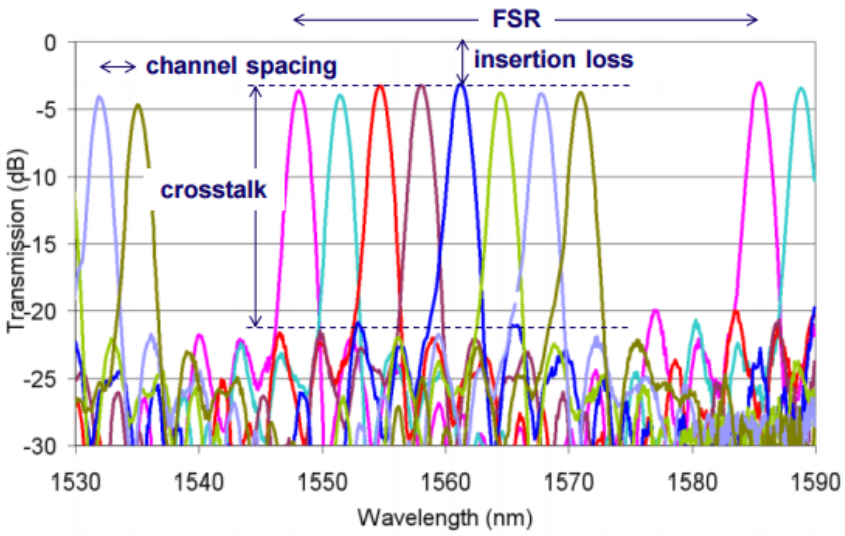

Figure 5.2: Spectrum measures of AWG [35].

First of all, it was crucial to choose the right central wavelength and consequently, the best FSR to match the desirable wavelengths. Then, it was important to have a crosstalk of around -30 *dB* to have low interference between channels. Beyond this, it was also relevant to take care with the non-uniformity of the channels. Moreover, the last factor, was the size of these components that should be as reduced as possible. It is important to refer that the software does not support simulations above 1600 *nm* so part of these AWG's response cannot be seen.

Initially, an AWG 1x4 was designed. The aim of this AWG is to separate the four channels of the downstream direction so the ONU will receive the respective wavelength. The following Table 5.2 demonstrate all the parameters used to perform this AWG 1x4. The chosen central wavelength was 1.5963 μm that is the mid-point of the downstream channels. Then, the channel spacing was set as 100 *GHz*. In order to avoid replicas on the upstream band an FSR of 1526 *GHz* was chosen. The FSR value was carefully studied because as it is increased, the size of the component will also get bigger, that is not what is pretended.

Parameters	Value
Number of inputs	1
Number of outputs	4
Central wavelength	1.5963 μm
Channel spacing	100 GHz
Free spectral range (FSR)	1526 GHz
IO waveguide width	3.0 μm
IO waveguide pitch	5.5 μm
Array waveguide width	1.5 μm
Gap between array waveguides at FPR	0.6 μm
Array acceptance factor	2.2
Chirp factor	0.0

Table 5.2: AWG 1x4 design parameters

With these parameters, the final response of the simulation is in the following Figure 5.3. The different lobes can be seen with different colours that represent the four channels. The lobes from the right side match the downstream wavelengths as desired. The others ones are replicas that appeared because of the determined FSR . The insertion loss is 1.6 *dB*, and the cross talk between adjacent channels is around -20 *dB*.

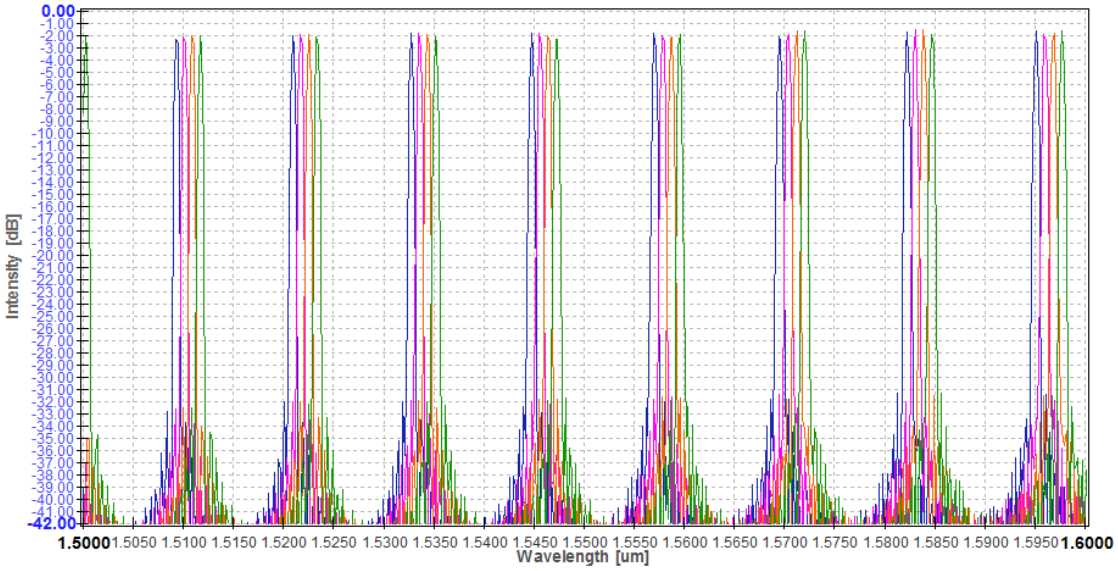

Figure 5.3: Spectrum of the AWG 1x4 using Aspic^{TM} simulator.

This section presents the next step in designing the Multiplexer / Demultiplexer. At this point, an AWG 1x2 will be design whose purpose is to filter the downstream and upstream channels of the transceiver. So, this AWG is working as a filter that rejects all the undesired copies from the previous one. The parameters used to design this AWG are exposed in Table 5.3

In this case, the central wavelength is 1.5932 μm that is almost the mid-point of the upstream channel. This value was optimised to obtain the two lobes covering the four channels of the downstream and also the upstream. Like it was said, the aim of this AWG is to cover the upstream and downstream channels (C and L bands) so, for that, the chosen channel spacing was 765 *GHz*.

Parameters	**Value**
Number of inputs	1
Number of outputs	2
Central wavelength	1.5932 μm
Channel spacing	765 GHz
Free spectral range (FSR)	6900 GHz
IO waveguide width	3.2 μm
IO waveguide pitch	6.5 μm
Array waveguide width	0.5 μm
Gap between array waveguides at FPR	0.6 μm
Array acceptance factor	2.2
Chirp factor	0.0

Table 5.3: AWG 1x2 design parameters

The results of the simulation of this AWG are shown on the following Figure 5.4, where the blue curve is filtering the four channels of the upstream direction and the magenta one, is covering the downstream channels. These filters in Figure 5.4 have, approximately, 1.5 *dB* of insertion loss and -25 *dB* of crosstalk.

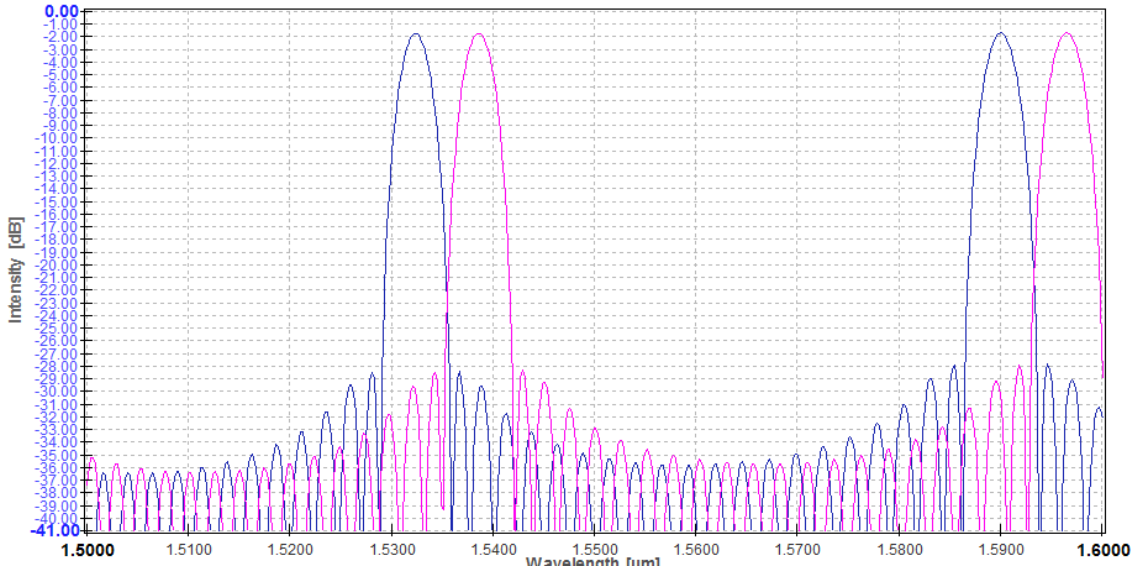

Figure 5.4: Spectrum of the AWG 1x2 using Aspic^{TM} simulator.

Figure 5.5 depicts both responses of the two AWGs as a system. One can notice that the rejection of the undesirable copies of the first AWG 1x4 was successfully done, where it can seen the four channels of the downstream with the spotlight. The intensity of undesired copies is considered insignificant since it measures -30 dB.

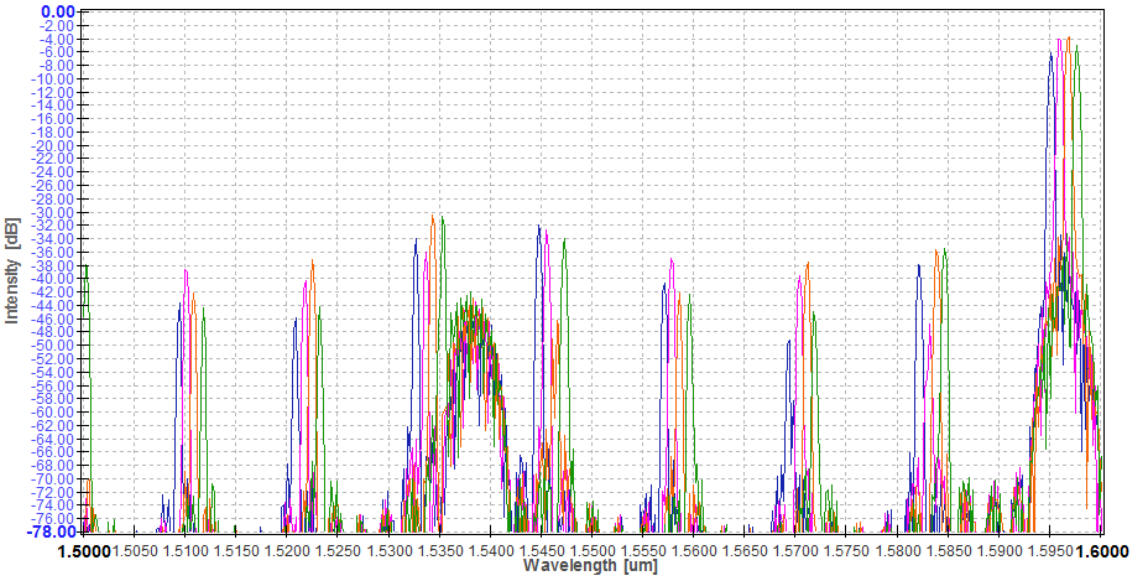

Figure 5.5: Spectrum of both AWGs using Aspic^{TM} simulator.

5.3 Mask Layout of the Transceiver

As the name suggests this section will show the design implementation of the transceiver using PhoeniX Software's OptoDesigner. This software supports the PDK of FhG-HHI's foundry, so it contains libraries with the necessary building blocks to construct the transceiver.

To do so, several rules have to be obeyed according to the Design Rules of the chosen foundry in order to decide the best way to fit it in the available area.

First of all, the design must have to be placed in a 6 *mm* x 4 *mm* user area. Then, other general rules are essential to take into account. Concerning about the distance between adjacent waveguides, it must be more than 1.5 μm. The correct position of the components like lasers, amplifiers, and other components, is also a rule to be followed, where the optical inputs need to be perpendicular to the major flat. Another rule is about the minimum radius for the E1700 arc waveguides, where it should be 150 μm and the lowest width for the straight passive waveguides is 1 μm. All this information is available in the Design Manual from the foundry [31]. The software also offers a design rule check (DRC) verification that performs some tests to avoid problems and to confirm that the solution proposed does not have errors.

5.3.1 Transmission Block

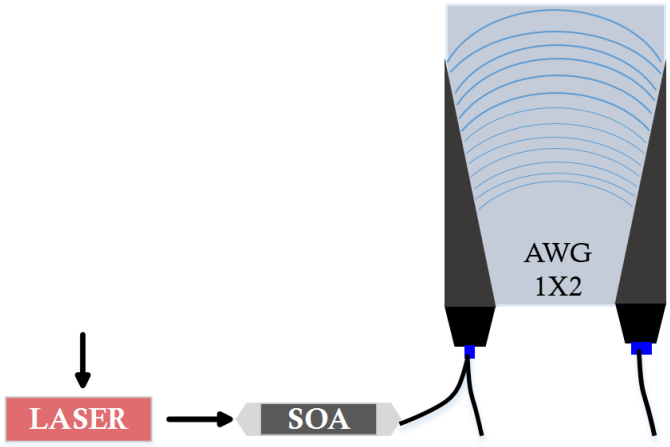

Figure 5.6: Diagram of the transmission block.

Figure 5.6 presents the transmission block of the transceiver. This section is composed by the DFB laser, the SOA and the 1x2 AWG.

The DFB laser is a building block that contains six ports, two are optical ports and the

others four are electrical ports. One of these electrical ports holds the carrier signal which is going to be direct modulated. The wavelength can be tuned by changing the temperature of the laser cavity. Right after the laser comes the SOA. The aim of this amplifier is to provide a signal boost. It has four ports, two optical and another two electrical. One of the electrical port is used to inject current for their operation. The third and last block is the 1x2 AWG. This component separates the C and L bands, to distinguish the upstream and downstream directions.

5.3.1.1 Mask Layout of the Transmission

The transmission block from the mask layout implementation is shaded in the following Figure 5.7. The DC pads do not appear in this Figure to provide a better view of the layout.

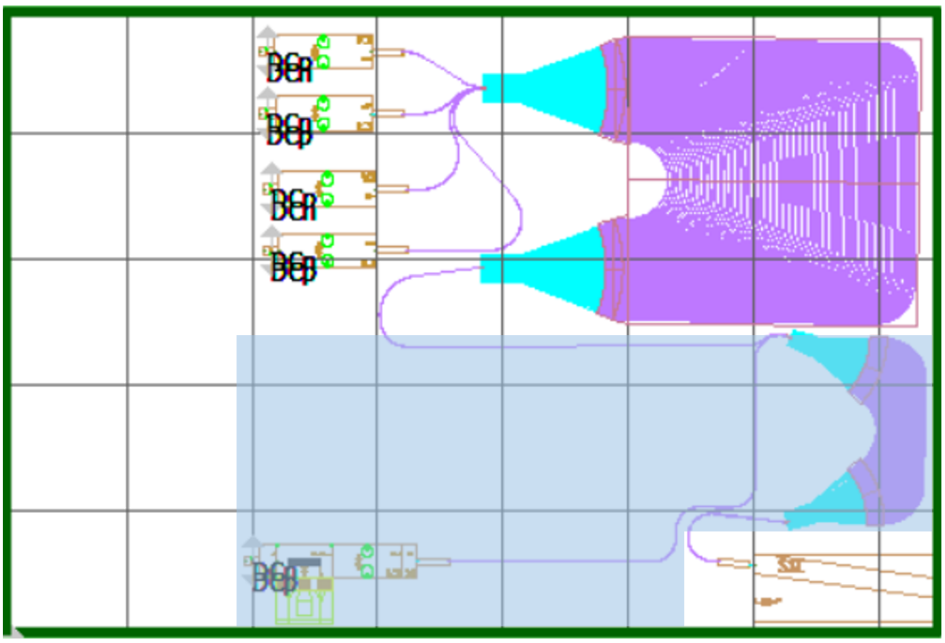

Figure 5.7: Transmission block of the mask layout (shaded).

At the bottom left part of the chip, the laser, and SOA are installed. The foundry provides a laser with and without joints to couple among the waveguides. For this case, it was chosen a laser which the joints are not included because it provides lower size. This choice was also made for the SOA block.

The laser, the SOA, and an active isolation to optically connect to the active components were placed. Right after, there is a block whose function is to transit from an E200 to an E1700 cross section. This is required, since the cross section from the lasers, amplifiers and

photodetectors is the E200 one and, as it was presented in Chapter 4, the E1700 waveguides offers lower propagation loss comparing to the E200 and it is always a good practice to mitigate the losses in a transceiver.

Then, there is a connection between the transition block till the 1x2 AWG. This path was done using passive waveguides. In this particular case, the straight and arc ones were used.

The final block for this transmission part is the 1x2 AWG. The path referred before, is connected to one port from this block. The location of this block was carefully studied since the input of this multiplexer connect to the Spot Size Converter (SSC).

Concerning the SSC, the purpose of this block is to couple light in and out of the chip. One of the main rules about this block is that it needs to be on the edge of the mask, as it shows in Figure 5.7. Looking with more attention, it can be seen that this block is angled by 7 degrees to reduce the reflections on chip to fiber coupling.

5.3.2 Reception Block

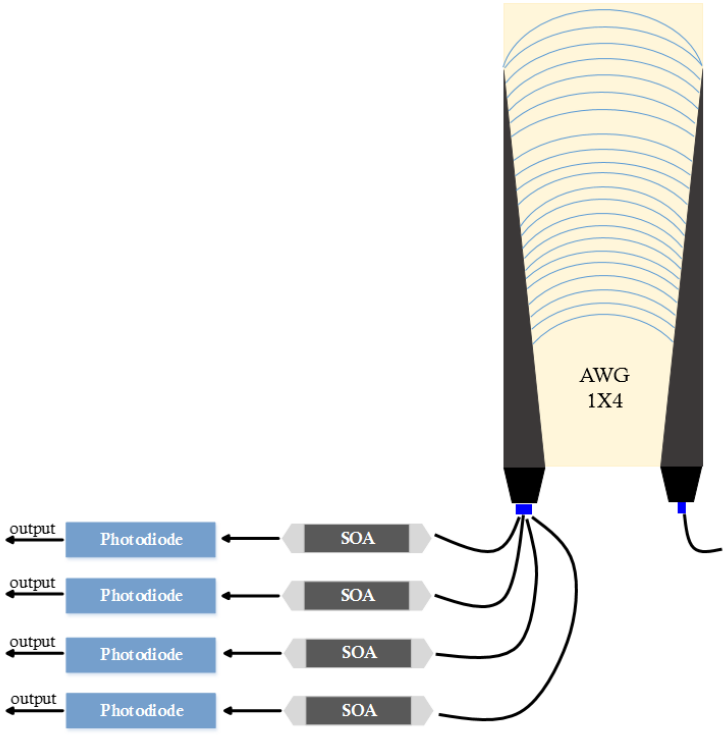

Figure 5.8: Diagram of the reception block.

The reception block starts with a 1x4 AWG. This AWG acts as a demultiplexer whose functionality was presented in Section 5.2.2. The input port is connected to the other AWG presented in the transmission block. Then, the four output ports are combined to a SOA, which is used as pre-amplification. The amplifier is a good policy to improve the signal reception, as it was demonstrated in Chapter 4 (Section 4.6.1). Lastly, for the reception of the signal, there are four photodetectors, PINs.

The Figure 5.8 presents the receiver block of the transceiver. In the diagram, one can see the main blocks that are the 1x4 AWG, the four SOA and four PINs.

5.3.2.1 Mask Layout of the Reception

The mask layout of the reception part is shaded in Figure 5.9. The blocks of the transceiver that occupy more area are, without a doubt, the AWGs, in particular the 1x4 AWG. Since this one is the biggest component, the location of it was chosen to be on the top right of the chip. The four outputs have the needed waveguides routes to connect to each amplifier. Before connecting to the amplifier a transition between the E1700 cross section to the E200 one is required.

The four photodiodes were placed after each amplifier, where they are all parallel and aligned to give a better uniformity of the space.

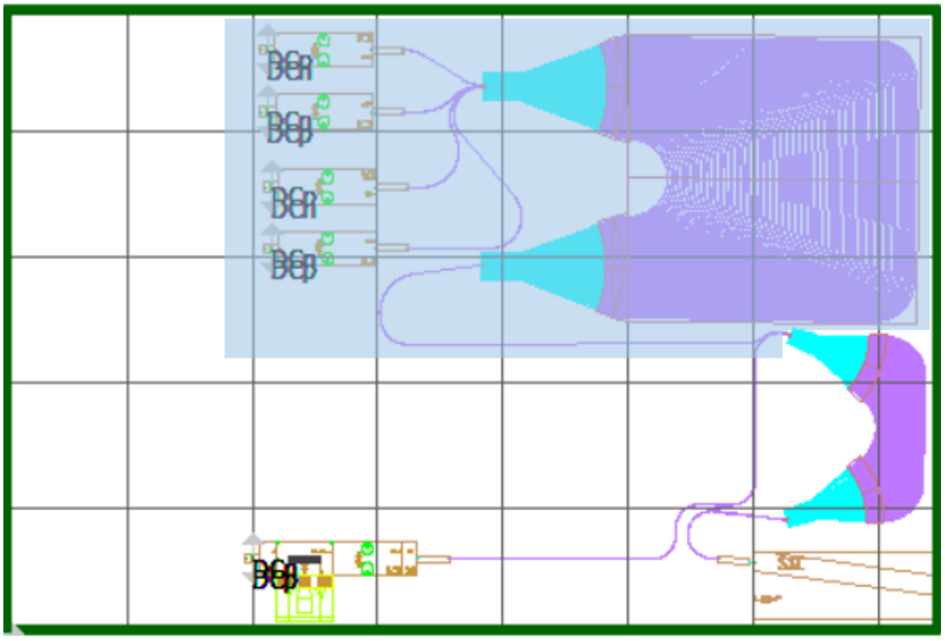

Figure 5.9: Reception block of the mask layout (shaded).

5.4 Final Mask Layout of the Transceiver

The overall transceiver mask layout was completed in the previous sections, but for the final mask, it was necessary to introduce some electrical connections in particular components. These electrical pads were done using DC interconnects whose form is like a square and the size is 100 μm^2. One consideration to take into account is the space between the DC pads that should be at least 100 μm due a physical limitation required by the bonding machine of the department.

Firstly, it was required to include pads for the SOAs. Each SOA has two electrical DC ports. Moreover, 4 more pads were necessary for the laser, two DC pads and the other two were RF pads since this architecture is intended to support 25 Gb/s (12.5 GHz), so there are RF pads support high frequencies. Finally, two more DC pads to each PIN photodiode.

The pads were placed on the left side of the chip, all aligned in parallel and with 100 μm of minimum space.

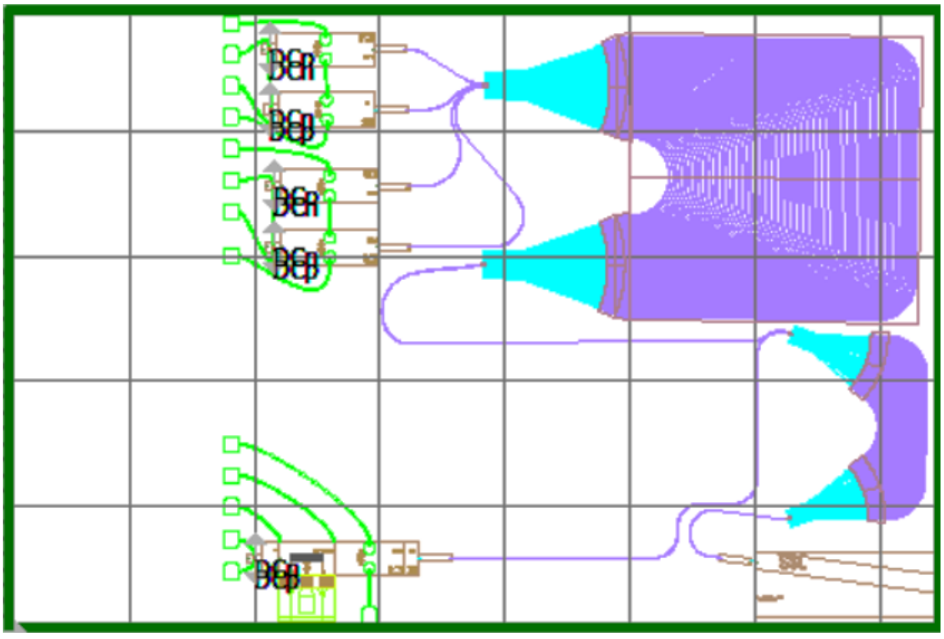

Figure 5.10: Mask layout of the ONU transceiver.

The last step in the design flow is the generation of the mask layout. To do that, theDRC was run. Since all the rules were obeyed and no problems were reported, it was possible to perform the exportation of the design where several files are generated. One of them is the GDS file; that is the presented in the following Figure 5.11.

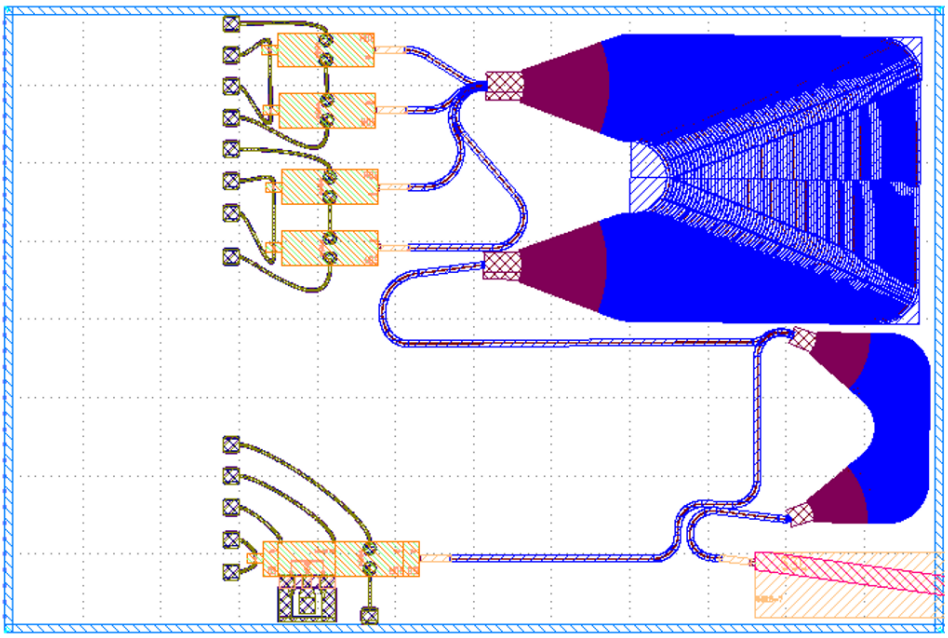

Figure 5.11: GDS mask of the ONU transceiver.

Chapter 6

Conclusions and Future Work

This chapter is divided in two sections. Section 6.1 presents the conclusions of this dissertation. And finally, section 6.2 expose suggestions for future work.

6.1 Conclusions

Nowadays it is required higher bandwidth, more split ratio and longer reach in the networks. There is a necessity to find new modulation formats to achieve this concept since, the NRZ-OOK is no longer sufficient. In this dissertation, simulations were done concerning the modulation format's topic. A brief overview of PAM format was outlined and the comparisons between NRZ-OOK and 4-PAM were done. Simulations have shown that the spectral efficiency and the dispersion tolerance are better in the 4-PAM format. This modulation format is more suitable candidate for the NG-EPON architecture.

PICs represent a trending solution for optical communications following the increasing demand for higher data bandwidths Looking at future cost trends, it is predicted that the adoption of PIC technology yields significant equipment cost savings as well as lower power consumption. However, the industry still needs to invest their efforts on research and development in order to achieve profitable mass production.

This dissertation is a contribute for the development of this technology and proposes an implementation of a photonic integrated circuit for the next generation of Ethernet passive optical network (NG-EPON).

In a early stage for the development of this work, it was essential to understand the basic concepts of the optical components, so a study of the major operational principles was done to every block that used to perform the proposed transceiver architecture.

The next step was devoted to a characterization of the components from the FhG-HHI foundry to understand the performance of each block and to analyse their behaviour. This work was done under a powerful toolkit from VPIphotonics^{TM} which allows design InP-based photonic integrated circuits from FhG-HHI.

The last step achieved the main goal of this dissertation: the proposal and design of the transceiver. It started with an overall view of the architecture based on a block diagram. After that, the design and modulation of the AWGs took place, using the Aspic^{TM} simulator. Then, the design of the architecture was shown divided in transmission and reception blocks, for a better understanding.

As a final result, a transceiver for the ONU side in NG-EPON context was presented. It has a tunable approach with four channels spaced by 100 GHz supporting a four-level modulation (4-PAM). The final layout is ready to be produced in the foundry.

6.2 Future Work

As follow up to this work the following topics may be interesting to pursue:

- The overall transceiver could be analysed and tested in a system level simulation to extend the understanding and potential of the architecture.
- As seen in this work the AWGs are a massive component that occupies most of the available area of the PIC. Thus, investing more time in optimizing them could bring more value to this work.
- Further laboratory work with the full system can provide more information about how the architecture works as a all.
- Manufacture of the proposed PIC could be done. A design and implementation of its packaging could be also addressed.

Bibliography

[1] Philippe Chanclou, Stéphane Gosselin, J Fernandez Palacios, V Lopez Alvarez, and Evi Zouganeli. Overview of the Optical Broadband Access Evolution: A Joint Article by Operators in the IST Network of Excellence e-Photon/One. *IEEE Communications Magazine*, 44(8):29–35, 2006.

[2] Chang-Hee Lee, Sang-Mook Lee, Ki-Man Choi, Jung-Hyung Moon, Sil-Gu Mun, Ki-Tae Jeong, Jin Hee Kim, and Byoungwhi Kim. WDM-PON experiences in Korea [Invited]. *Journal of Optical Networking*, 6(5):451–464, 2007.

[3] M. Smit. An introduction to InP-based generic integration technology. *Semiconductor Science and Technology*, 29(8), June 2014.

[4] Ivica Cale, Aida Salihovic, and Matija Ivekovic. Gigabit Passive Optical Network-GPON. In *29th International Conference on Information Technology Interfaces*, pages 679–684. IEEE, 2007.

[5] David Law. *IEEE 802.3 Ethernet Working Group Communication.* March 2015.

[6] CommScope. *GPON - EPON Comparison.* White Paper, October October 2013.

[7] Hiroyuki Ishii, Yasuhiro Kondo, Fumiyoshi Kano, and Yuzo Yoshikuni. A Tunable Distributed Amplification DFB Laser Diode (TDA-DFB-LD). *IEEE Photonics Technology Letters*, 10(1):30–32, 1998.

[8] Cedric F. Lam. *Passive Optical Networks: Principles and Practice.* Academic Press, 2007.

[9] William Shieh and Ivan Djordjevic. *OFDM for Optical Communications.* Academic Press, 2009.

[10] VPIphotonics. Introduction to Optical Transmitters Tx1 - Lecture Series. Technical report, Univeristy Program, Photonics Curriculum Version 8.0.

[11] Harry J.R. Dutton. *Understanding Optical Communications.* Prentice Hall PTR New Jersey, September 1998.

[12] G. P. Agrawal. *Fiber-Optic Communication Systems.* John Wiley & Sons, Inc., 2002.

[13] M. J. Connelly. *Semiconductor Optical Amplifiers,.* Springer Science & Business Media, 2007.

[14] Riyam A Johni, David I Forsyth, and Kanar R Tariq. Effects on Semiconductor Optical Amplifier Gain Quality for Applications in Advanced All-optical Communication Systems. *Research Journal of Applied Sciences, Engineering and Technology*, 7(16):3414–3418, 2014.

[15] John M. Senior. *Optical Fiber Communications: Principles and Practice.* Pearson Education, third edition edition, 2009.

[16] Meint K. Smit and C. Van Dam. PHASAR-based WDM-devices: Principles, Design and Applications. *IEEE Journal of Selected Topics in Quantum Electronics*, 2, 1996.

[17] Herbert Venghaus. *Wavelength filters in fibre optics*, volume 123. springer, 2006.

[18] Hari Singh Nalwa. *Photodetectors and fiber optics,.* Elsevier, 2012.

[19] VPIphotonics. Introduction to Optical Receivers Rx1 - Lecture Series. Technical report, Univeristy Program, Photonics Curriculum Version 8.0.

[20] Leonid G. Kazovsky, Ning Cheng, Wei-Tao Shaw, David Gutierrez, and Shing-Wa Wong. *Broadband Optical Access Networks.* John Wiley & Sons, 2011.

[21] M. Smith J. Van der Tol, M. Hill. *Moore's law in photonics*, volume 6. Wiley Online Library, 2012.

[22] Infinera. Photonic Integrated Circuits - A Technology and Application Primer. White Paper, 2005. Accessed: 2016-10-11.

[23] JePPIX. Platforms capabilities. `http://www.jeppix.eu/platforms.html`. Accessed: 2016-11-01.

[24] JePPIX. Joint European Platform for InP-based Photonic Integrated Components and Circuits. http://www.jeppix.eu. Accessed: 2016-10-11.

[25] JePPIX. The road to a multi-billion Euro market in Integrated Photonics. http://www.jeppix.eu/document_store/JePPIXRoadmap2015.pdf, 2015. Accessed: 2016-10-11.

[26] Sugianto Trisno. Design and analysis of advanced free space optical communication systems. 2006.

[27] K. Kikuchi. Coherent Optical Communications: Historical Perspectives and Future Directions. *Springer*, 6:11–50, January 2010.

[28] Taissir Youssef Elganimi. Performance Comparison between OOK, PPM and PAM modulation schemes for free space optical (FSO) communication systems: analytical study. *International Journal of Computer Applications*, 79(11), 2013.

[29] Fraunhofer Heinrich Hertz Institute, HHI. https://www.hhi.fraunhofer.de/en/fraunhofer-hhi/about-us.html. Accessed: 2016-09-08.

[30] VPItoolkit^{TM} PDK HHI - Overview. http://www.vpiphotonics.com/Tools/PDK_HHI/. Accessed: 2016-09-08.

[31] PARADIGM. EUROPIC Design Manual, July 2014.

[32] Ian Armstrong, Ivan Andonovic, and Anthony Kelly. Semiconductor optical amplifiers: performance and applications in optical packet switching [invited]. *Journal of Optical Networking*, 3(12):882–897, 2004.

[33] Tiago Manuel Coelho Morgado. Photonic Integrated Circuits for NG-PON2 Networks. Master's thesis, University of Aveiro, July 2016.

[34] Aspic Advanced Simulator for Photonic Integrated Circuits. http://aspicdesign.altervista.org/. Accessed: 2016-08-17.

[35] Arrayed Waveguide Gratings. http://www.jeppix.eu/education/2015/ETRI/AWG_XL.pdf. Accessed: 2016-11-10.